
3. TRANSPORT OF RADIONUCLIDES IN THE ARCTIC SEAS

D. Layton^a, P. Vaughn^b, L. Yarrington^b, R. Maxwell^a, R. Preller^c, J. Bean^b, J. Carroll^d,
M. Fuhrmann^e, I. Rigor^f, and W. Tucker^g

^aLawrence Livermore National Laboratory, Livermore, CA

^bSandia National Laboratories, Albuquerque, NM

^cNaval Research Laboratory, Stennis Space Center, MS

^dInternational Atomic Energy Agency, Marine Environment Laboratory, MONACO

^eBrookhaven National Laboratory, Upton, NY

^fPolar Science Center, University of Washington, Seattle, WA

^gU.S. Army Cold Regions Research and Engineering Laboratory, Hanover, NH

Three sets of factors control the spatial and temporal changes in the concentration of a radionuclide released into the Arctic Ocean. The first set involves the nature and magnitude of the releases from various sources; the second set concerns the physical, chemical, and biological properties of ocean waters transporting the radionuclides; and the final set involves radionuclide-specific factors, such as radioactive decay and sediment-water partitioning. Section 2 addresses source-term-related factors to estimate potential releases of radionuclides from dump sites in the Northwest Pacific Ocean and the Kara Sea as well as from riverine sources. This section presents a methodology for predicting concentrations of radionuclides in Arctic waters adjacent to Alaska. The methodology uses radionuclide source terms as inputs to models that simulate the movement of radionuclides in Arctic waters. In addition to actual field measurements, subsequent sections will then use the results of the transport modeling to assess the potential risks to Alaskan populations and aquatic ecosystems.

3.1 SELECTION CRITERIA FOR RADIONUCLIDE TRANSPORT MODELS

Key considerations in selecting and implementing models to simulate the transport of radionuclides released into the Arctic Ocean are the spatial and temporal scales required to assess the potential health and ecological impacts of the releases. Basically three spatial scales can be addressed: global, regional, and local. This study is a regional-scale analysis that deals with radionuclide transport in the Arctic Ocean and the potential risks to Alaskan populations from dietary exposures to seafood. In contrast, a global-scale assessment of radionuclide releases is valuable in determining the magnitude of population exposures to radionuclides at low levels in seafood worldwide. A local-scale analysis would focus on a limited geographic region such as the Kara Sea. From a temporal perspective the model also must be able to trace the movement of nuclides in the Arctic Ocean for hundreds of years because of the slow leaching of radionuclides from submerged reactors. Such a model also must be able to complete simulations of radionuclide release scenarios or conduct sensitivity analyses in a reasonable amount of time.

Given these criteria, the RAIG used a compartmental model (CM) for the risk assessment. A compartmental model represents an ocean region as a series of linked compartments or boxes that encompass the entire volume of the region being assessed. Each compartment can exchange water with all compartments adjacent to it. Volumes of water on the order 10^{13} m^3 and larger (i.e., a single ocean compartment) are thus characterized by a single temperature, salinity, radionuclide concentration, sediment loading, sedimentation rate, etc. This extreme physical simplification is intentional to assure rapid, low-cost, easily run simulations suitable for sensitivity or other repetitive studies carried out by the RAIG.

Compartmental models have been used for many years to assess the potential consequences of radionuclides releases to ocean waters. For example, Clark and Webb (1981) used a model consisting of 17 compartments to assess radionuclide releases to northern European waters. Their basic model formulation and transport equations have been adopted in other studies of radionuclide releases to the marine environment (e.g., Evans, 1985; Hallstadius et al., 1987; Nielsen et al., 1995). Nielsen et al. (1995) developed a comprehensive model for the Northeast Atlantic coastal waters to simulate discharges of radionuclides from the nuclear reprocessing plants at Sellafield, UK, and La Hague, France. Alternative modeling approaches such as general circulation models, turbulent boundary layer models, regional eddy-resolving models, or coastal process models have extensive computational requirements and, when applied to a risk assessment on the scale of the Arctic Ocean, computational requirements become prohibitive.

3.2 SIMULATING RADIONUCLIDE TRANSPORT IN THE ARCTIC OCEAN

The basic compartmental structure for the model represents a vertical column that extends from a sediment layer to the water surface (Figure 3-1). The water portion of the column is represented by either a two-box configuration, where a surface compartment is underlain by a lower compartment, or by a single box for shallow areas such as shelf regions. A well-mixed sediment layer resides at the bottom of each water column. Water exchanges between adjoining compartments occur both in the vertical and horizontal domains for the two-box vertical configuration, but in the single-box case only horizontal water exchanges occur.

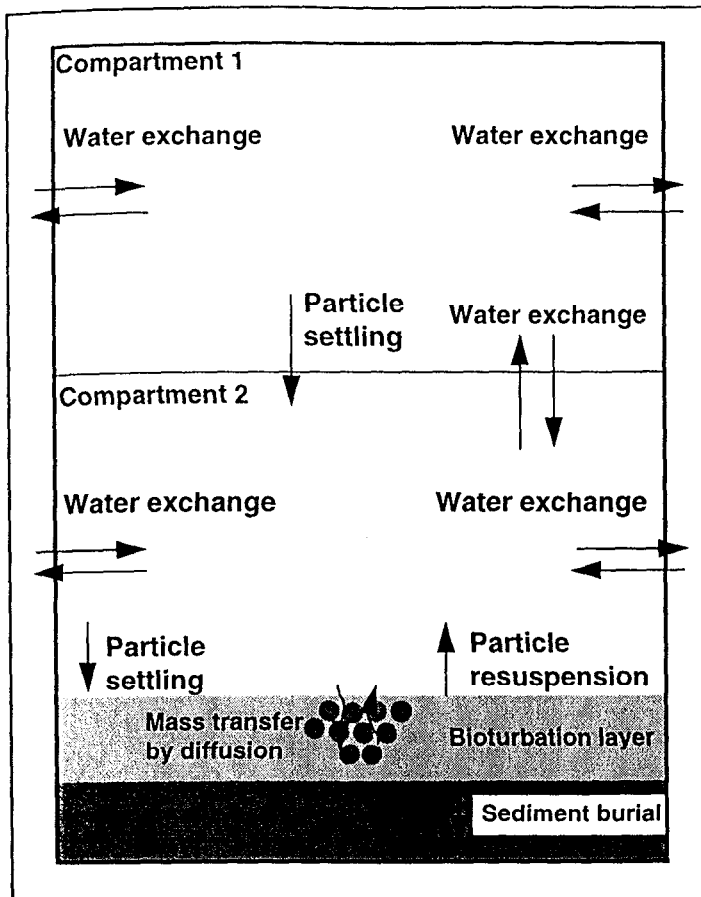


Figure 3-1. Basic compartmental structure for simulating the advective transport of radionuclides in water between two stacked water compartments as well as adjacent water compartments. Radionuclide exchanges also occur between a bottom water compartment and a sediment layer via particle settling and resuspension and pore-water diffusion.

Transport of radionuclides in the water compartments is governed by water flows between compartments as well as the vertical deposition of particle-bound nuclides to sediment. A sediment compartment is used to represent the accumulation of radionuclides in an active sediment layer as a result of resuspension, bioturbation, pore-water diffusion, and burial. Losses of radionuclides within each compartment also occur via radioactive decay. The relative importance of the water- and sediment-based transport processes for a given radionuclide is a function of its physicochemical properties as well as the characteristics of the marine environment that serves as the transport medium.

The following subsection presents an overview of the mathematical equations used to simulate radionuclide transport mechanisms and to predict radionuclide concentrations within individual model compartments. To provide insight on which of the transport mechanisms are most important, follow-on subsections provide explanations of the potential significance of the sediment/water distributions of the nuclides, the role of sediment deposition/resuspension, and finally, the transport of sediment-bound nuclides by near-shore ice.

3.2.1 Mathematical Formalism for the Compartmental Model

The governing equation for the total activity of a radionuclide in the i th compartment is given by

$$\frac{dA_i}{dt} = \sum_{j=1}^n k_{ji}A_j - \sum_{j=1}^n k_{ij}A_i - \lambda_d A_i + Q_i(t), \quad (3-1)$$

where A_i is the total activity (Bq) for compartment i in both dissolved and particulate phases. The terms k_{ij} (rate constant for radionuclide transfers from compartment i to j) and k_{ji} (rate constant for radionuclide transfers from compartment j to i) represent the rate constants (in 1/yr) for intercompartment exchanges for the n compartments in the system. Additional terms address radioactive decay (λ_d , in 1/yr) and time-varying sources (Q_i) within individual compartments (Bq/yr). These equations simply state, in mathematical terms, that the radioactivity (or mass) of radionuclide entering a given compartment minus the radioactivity (or mass) leaving a compartment must equal the radioactivity (or mass) of the radionuclide that accumulates in the compartment. The transfer rate constant for the volumetric exchange between adjoining horizontal compartments i and j is calculated from

$$k_{ij} = \frac{F_{ij}}{V_i}, \quad (3-2)$$

where F_{ij} is the volumetric flow rate of water from compartment i to compartment j (m^3/yr) and V_i is the volume (m^3) of the i th compartment. The rate constant representing both water exchange and the settling of particle-bound radionuclides from the top water compartment to the lower water compartment in a two-layer water column is estimated from

$$k_{ij} = \frac{F_{ij}}{V_i} + \frac{A_s S_v (1 - \phi_{dw})}{V_i}, \quad (3-3)$$

or alternatively,

$$k_{ij} = \frac{F_{ij}}{V_i} + \frac{K_d S_v S_L}{h(1 + K_d S_L)}, \quad (3-4)$$

where

$$\phi_{dw} = \frac{1}{(1 + K_d S_L)}, \quad (3-5)$$

and

K_d	=	sediment/water distribution of radionuclide, m^3/kg ;
S_L	=	mass loading of particulate matter in water, kg/m^3 ;
S_v	=	sedimentation rate of suspended particles, m/yr ;
h	=	depth of ocean compartment, m ;
A_s	=	surface area of bottom sediments, m^2 ; and
ϕ_{dw}	=	fraction of radionuclide inventory in a seawater compartment that is dissolved, unitless.

Exchanges of a radionuclide between a benthic water compartment and a sediment compartment are simulated using rate constants that represent the movement of radionuclides from water to sediment compartments and from sediment to the overlying water compartment. The primary transport mechanisms for water-to-sediment transfer of a radionuclide are the deposition of particle-bound nuclides and the diffusion of a dissolved radionuclide from seawater to sediment pore water under a concentration gradient. For water-to-sediment transfers, the rate constants are calculated (after Gobas et al., 1995) as

$$k_{ij} = \frac{A_s T_m \phi_{ds}}{V_i} + \frac{A_s S_v (1 - \phi_{ds})}{V_i}, \quad (3-6)$$

where

$$\phi_{ds} = \frac{1}{(1 + K_d \rho_s (1 - \theta_s))}, \quad (3-7)$$

and

ϕ_{ds}	=	fraction of radionuclide inventory in the sediment compartment that is dissolved, unitless;
T_m	=	mass-transfer coefficient for diffusive transfers of a radionuclide between pore water in sediment and the water column, m/yr ;
θ_s	=	porosity of sediment layer, unitless; and
ρ_s	=	density of sediment particles, kg/m^3 .

Transfers from sediment to overlying water occur via diffusion of soluble species from pore water to overlying water and by resuspension of sediment. The rate constant for these processes is expressed as

$$k_{ij} = \frac{A_s T_m \phi_{ds}}{V_i} + \frac{\frac{R_s}{(\rho_s (1 - \theta_s))} (1 - \phi_{ds})}{V_i}, \quad (3-8)$$

where R_s is the resuspension rate of sediment, kg/yr . The resuspension rate can be calculated as the difference between sediment burial and deposition, or

$$R_s = A_s(S_v S_L - B_r \rho_s (1 - \theta_s)), \quad (3-9)$$

where B_r is the burial rate of sediment, m/yr.

3.2.2 Radionuclide Partitioning Between Sediment and Seawater

Particulate matter, also known as sediment, exists in natural marine systems both suspended in seawater and deposited on the seafloor. In response to physicochemical reactions that occur in seawater, contaminants introduced into a marine system will be partitioned between particles and seawater (Duursma and Carroll, 1996). In most transport models, a simple parameter known as the distribution coefficient (K_d) is used to predict the quantities of a contaminant dissolved in seawater and attached to particles (e.g., Eqs. 3-5 and 3-7). The distribution coefficient is defined as

$$K_d = \frac{C_s}{C_w}, \quad (3-10)$$

and is based on the assumption that the concentrations of a contaminant in water (C_w , in Bq/m³) and particulate matter (C_s , Bq/kg, dw of material) are at steady-state, or equilibrium conditions. As K_d increases, more contaminant is associated with particles and hence contaminant behavior in water becomes more dependent on the fate and transport of particles.

The K_d concept assumes that adsorption is the uptake mechanism by which a contaminant attaches to particles. Adsorption is generally considered to be a surface-related chemical attachment process that is completely reversible. Distribution coefficients in marine systems are typically determined through three types of procedures:

- (1) Measurements of elemental concentrations in seawater are compared with either a) measurements of elemental concentrations for marine sediments or b) estimates of the exchangeable fraction of the total elemental concentrations for particles not previously exposed to seawater. This approach provides global estimates of K_d values, such as is presented in IAEA (1985) for coastal waters.
- (2) Local measurements are conducted of specific contaminants associated with marine particles and seawater. While this approach provides site-specific K_d values, there is limited certainty that the particles have remained in contact with the seawater from which the contaminant was initially sorbed.
- (3) Laboratory and field investigations of contaminant sorption dynamics are performed in batch, isotherm or flow-through column (more appropriate for ground water) experiments. Advantages of the laboratory approach include the ability to determine sorption and desorption kinetics and to evaluate effects of changing environmental conditions. This provides better predictive capabilities, however, issues of maintaining the original properties of the sediment/water matrix and the representativeness of experimental protocols to nature remain concerns in this approach.

Mechanistically and in the strictest sense the definition of K_d (Eq. 3-10) may not be completely appropriate. For example, mechanisms other than adsorption can result in a contaminant moving from seawater to particulate matter, including:

- Precipitation directly from solution;
- Surface-mediated redox reactions and precipitation;
- Ion exchange;
- Isotope exchange;
- Co-precipitation; and
- Organic/metabolic processes.

Furthermore, the state of the art for mechanistically describing adsorption uses models of reactions of species in solution with species on mineral surfaces. These models, known as surface-complexation models, provide descriptions (generally by use of a geochemical speciation code) of sorption behavior as a function of pH and ionic strength. The models do not easily address complex mixtures of minerals and organic matter, as are found in natural seawater systems. As a necessary simplification, transport modelers use the K_d approach in their models to predict distributions of a contaminant between sediment and seawater.

Data on the sediment-water partitioning of waste-related radionuclides exist for the Kara Sea (Povinec et al., 1996; Fuhrmann et al., 1996; Duursma and Carroll, 1996; Cochran et al., 1996; Carroll et al., 1995). These site-specific K_d estimates provided by batch laboratory and field experiments may be compared to earlier K_d values compiled for coastal waters by the International Atomic Energy Agency (IAEA, 1985) (Table 3-1). Note that the site-specific K_d values are lower than the generic values recommended by the IAEA (1985). This is not surprising because it is well known that particulate matter collected from different coastal marine waters varies in composition (e.g., organic matter content, clay content, grain size, etc.). The site-specific K_d values reflect the unique composition of Kara Sea sediment.

Table 3-1. Sediment-water distribution coefficients for Am, Cs, Pu, and Sr for Kara Sea sediments.

Source	Radionuclide			
	Am	Cs	Pu	Sr
	Distribution Coefficients m^3/kg (unitless) ^a			
Povinec et al. (1996) ^b	10 - 400 ($0.1 - 4 \times 10^5$)	0.03 - 1 ($.3 - 10 \times 10^2$)	60 (6×10^4)	0.01 - 3 ($.01 - 3 \times 10^2$)
Cochran et al. (1996)	100 (1×10^5)	0.2 (2×10^2)		
Fuhrmann et al. (1996) ^c	—	0.3 (3×10^2)		0.004 (4×10^0)
IAEA (1985) ^d	2,000 (2×10^6)	3 (3×10^3)	100 (1×10^5)	1 (1×10^3)

^a The K_d value in units of m^3/kg (i.e., $Bq/m^3 \div Bq/kg$) must be multiplied by 1,000 to obtain a unitless value (i.e., assuming a density of water of $1,000 \text{ kg/m}^3$).

^b IAEA-MEL recommended K_d ranges for Kara Sea sediments based on sediment-water measurements.

^c Average of distribution coefficients reported for three Kara Sea sediments.

^d Recommended value for coastal waters.

The impact of K_d s in contaminant transport models further depends upon the mass of sediment in seawater. In a system with low-particle loading (even with a high K_d), uptake has less of an impact on contaminant concentrations simply because of the differences in mass of the two phases. However, in a system with high-particle loading, such as in fjords, the mass of solids can be large. In this case quantification of K_d and understanding its behavior as a function of particle loading becomes much more critical than in a system depleted of particles (Carroll and Harms, 1997). Estimating the distribution of each radionuclide between its dissolved and particulate phases in a unit volume of water will provide more clarification on the importance of particle-scavenging processes that control the accumulation of radionuclides in sediments (from Eq. 3-5). If the RAIG uses a particle loading of 5 mg/L (0.005 kg/m^3), less than 2% of the radioactivity of ^{137}Cs and ^{90}Sr in seawater will be associated with the particulate phase—even using the highest K_d s in Table 3-1. The most particle-reactive nuclide, ^{241}Am , would only have 9% of its activity associated with the water phase, based on the IAEA (1985) recommended K_d for coastal waters. But with the lower K_d measured for Kara Sea sediments ($\sim 100 \text{ m}^3/\text{kg}$), the fraction dissolved in water increases to 67%. For ^{239}Pu , the fractions dissolved in water range from 67 to 91% for particle loadings of 0.005 to 0.001 kg/m^3 . In the central Arctic Ocean, where suspended particle loadings are apparently much lower, the fraction of the particle-reactive nuclides in the dissolved phase would be even higher.

Implications of these findings to the transport modeling of radionuclides in the RAIG CM are the following. The calculated distributions of the dissolved/particulate fractions indicate that ^{137}Cs and ^{90}Sr will behave as conservative tracers in seawater, with very limited particle scavenging from the water column. The more particle-reactive radionuclides, ^{241}Am and ^{239}Pu , will be partially scavenged from the water column. As a result, their concentration levels will depend in part on spatial variations of particulate matter concentration along transport routes leading from the Kara Sea dumpsites to other Arctic waters. The RAIG performed more tests on the RAIG CM to evaluate model sensitivities to K_d values, which are discussed later in Section 3.

3.2.3 Sediment-Related Transport Processes

As demonstrated in the previous subsection, the existence of sediment in Arctic seas influences the fate and transport of particle-reactive radionuclides such as plutonium and americium. Sediment-related transport processes operating in the world's oceans include passive transport of particles by ocean currents, particle settling to deeper layers of the ocean or to the seafloor, particle resuspension from the seafloor by physical and biological mechanisms and permanent burial (Figure 3-1). The amount and composition of sediments varies from location to location on the seafloor in response to changes in the relative impact of each of the sediment-related processes. And yet, over very long timescales, the net impact of these processes is a loss of particles from the water column to the ocean floor. In conjunction with particle transport through the oceans, radionuclides themselves may undergo a variety of chemical transformations (Hamilton et al., 1994; Smith et al., 1994; Buesseler and Sholkovitz, 1987; Aarkrog et al., 1987). However, along with a net loss of particles to the seafloor, there will be an associated net loss of particle-reactive radionuclides (Smith et al., 1995; Hamilton et al., 1994).

In contaminant transport modeling, the simplest and most common approach used to account for the removal of radionuclides from seawater by particle deposition to the seabed is to employ a two-step approach. First, the distribution coefficient is used to predict the radionuclide concentration in seawater and on particles, then particles are removed from the system in accordance with the rate of particle deposition on the seabed. As previously discussed in this report, distribution coefficients have been determined for the Kara Sea. In the remainder of this section, information is presented on the distribution of particles and particle deposition rates in Arctic seas.

Although there are limited data on the levels of suspended particles in the Arctic Ocean, it is well-known that particle transport does not result in a uniform distribution of sediments throughout the Arctic Ocean. Ivanov (1994) reported values of 3 to 5 mg/L (0.003 to 0.005 kg/m³) for the Barents Sea and an average of 3.5 mg/L (0.0035 kg/m³) for the Kara Sea. Higher levels of suspended solids are associated with the bays along the Novaya Zemlya coastline, because of tidal and wave action that suspends sediments into the water column. Baskaran and Naidu (1995) reported particle loadings ranging from 0.03 to 0.96 mg/L (0.00003 to 0.00096 kg/m³) for the Chukchi Sea, but Bacon et al. (1989) measured concentrations of suspended matter below 0.01 mg/L (<0.00001 kg/m³) at an ice station located in the central Arctic basin (at 85° 50'N, 108° 50'W).

As a consequence of variable particle concentrations, particle deposition rates in Arctic seas range from mm/yr in the shallow Kara Sea to mm/ky in the deepest regions of the Arctic ocean. Radionuclides associated with dumped nuclear reactors will first be released into the Kara Sea. Hamilton et al. (1994) conducted a radiometric investigation of the Kara Sea sediments to determine the distribution of selected radionuclides in sediments and to estimate burial rates of sediment. They estimated burial rates by using ²¹⁰Pb as a natural tracer to date the age of sediments at different depths. The estimated rates (assuming that resuspension is negligible compared with deposition) ranged from 1.6 to 2.3 mm/yr, based on a sediment porosity of 0.86. These values are comparable to the sedimentation rates of 1 to 2 mm/yr estimated for Bylot Sound by Smith et al. (1994). Hamilton et al. also found that surficial sediments were well mixed in a shallow zone of a few centimeters in thickness.

The result of these variations in particle concentrations and deposition rates throughout the Arctic ocean is that sediments are non-uniformly distributed on the seabed. It is possible for contaminated sediments to be concentrated within specific subregions of the Arctic, such as on continental shelves (Baskaran et al., 1996; Cooper et al., 1995). If deposition is enhanced in regions

rich in biological resources, there is the potential for radionuclides to be more readily available for transfer into Arctic food webs. In compartmental models, a single particle concentration and deposition rate is assigned to each model compartment. As a result, the influence of smaller-scale variations in particle concentrations and deposition rates are not reflected in the results of the modeling exercises.

3.2.4 Role of Ice Transport

The following discussion provides perspective on sea ice-related processes and the importance of sea ice transport in relation to other radionuclide transport mechanisms operating in Arctic seas. The important mechanisms influencing radionuclide transport by sea ice are: (1) sediment incorporation into sea ice during sea ice formation; (2) radionuclide uptake into sea ice and by sea ice sediment; and (3) transport pathways for sea ice in Arctic seas. Given present limitations in knowledge of sea ice processes, simulations of sea ice and associated radionuclide transport were not included in the regional-scale compartmental model the RAIG team used. A simple comparison of water, sediment, and sea-ice transport, however, strongly suggests that the primary pathway for exchanging radionuclides among Arctic seas is water transport.

Direct observations have shown that sea ice incorporates and transports sediment (Nurnberg et al., 1994; Reimnitz et al., 1993; Kempema et al., 1989). The incorporation of sediments into sea ice is thought to occur primarily along the shallow circum-Arctic shelves at water depths generally less than 50 m, where levels of suspended sediments are highest because of the action of waves and currents on bottom sediments. One potential mechanism of sediment incorporation into ice is the scavenging of suspended sediment by frazil ice crystals in the water column (Pfirman et al., 1997). The interactions of ice with bottom sediments as well as wave overwashing of ice also may result in the incorporation of sediment in ice.

Mechanisms influencing the incorporation of radionuclides by sea ice are receiving more attention from investigators, primarily in response to recent concerns over Arctic nuclear waste. A comparison of recent data from ice formation experiments conducted at the Cold Regions Research and Engineering Laboratory (D. Meese, personal communication) and ^{137}Cs concentrations determined from Arctic sea-ice samples provide preliminary information to evaluate these mechanisms. These researchers collected samples of sea ice containing sediment and "clean ice" along a cruise transect from the Chukchi Sea to the North Pole. They determined high ^{137}Cs concentrations (5-73 Bq/kg dw) for the sea-ice sediment samples and low ^{137}Cs concentrations (<1 Bq/m³) for samples of non-sediment-rich or "clean ice" (Meese et al., 1997). Interestingly, the "clean ice" ^{137}Cs concentrations were even lower than ambient-seawater concentrations (2-15 Bq/m³; Ellis et al., 1995). Data from the ice-freezing experiments suggest that the ice rejects radionuclides during the freezing process in a manner similar to brine rejection.

The role that ice plays in the transport of radionuclides from the Kara Sea to other Arctic seas is further dependent upon the transport pathways for sediment-laden ice. Various techniques are under development to identify these pathways. One such method is to compare data on the sediment composition of sea ice with sediment samples from various coastal and ocean locations (Meese et al., 1997; Darby and Bischof, 1996). Analyses of iceborne sediment collected in the Beaufort and Chukchi Seas indicate that potential source areas are along the Russian shelves. An alternative technique involves the simulation of "backward" ice trajectories interpolated from current velocity fields determined from analyses of the movements of drifting ice buoys (Rigor and Colony, 1997). Simulations of the mean field of ice motion in the Arctic Ocean for the years

1979 to 1994 (provided by I. Rigor) suggest that the regional flow of ice is toward the Greenland Sea via the Fram Strait (Figure 3-2).

As previously noted, much of the data needed to establish the role of sea-ice transport as a distribution mechanism for radionuclides are still preliminary. Simple calculations comparing the relative magnitude of water, sediment, and ice transport from the Kara Sea provide some perspective on the relative importance of sea-ice transport as a conveyor of contaminated sediment to other Arctic seas. Rigor (personal communication) estimates that $2.1 \times 10^5 \text{ km}^2$ of sea ice are produced annually in the shallow waters of the Kara Sea. Based on an ice thickness of 2 m and $2.1 \times 10^4 \text{ km}^2$ of ice exported (i.e., 10% of the $2.1 \times 10^5 \text{ km}^2$ of ice formed in shallow waters), the annual volume of ice exported from the Kara Sea is approximately 40 km^3 . Assuming an elevated sediment loading of 100 mg/L (0.1 kg/m^3), 4×10^6 tonnes of sediment are exported annually to adjacent Arctic seas. The Kara Sea as a whole contains approximately $1.3 \times 10^5 \text{ km}^3$ of water and 4.6×10^8 tonnes of suspended sediment (using an average suspended sediment loading of 3.5 mg/L (0.0035 kg/m^3)). With a residence time of water in the Kara Sea of about 3.5 years (Pavlov et al., 1996), and a rate constant for water exchange of $0.29/\text{yr}$ (i.e., calculated as the inverse of the residence time or $1/3.5 \text{ yr}$), the approximate water ventilation rate is $3.8 \times 10^4 \text{ km}^3/\text{yr}$ (i.e., $0.29/\text{yr} \times 1.3 \times 10^5 \text{ km}^3$). The associated sediment load advected from the Kara Sea is 1.3×10^8 tonnes of sediment each year.

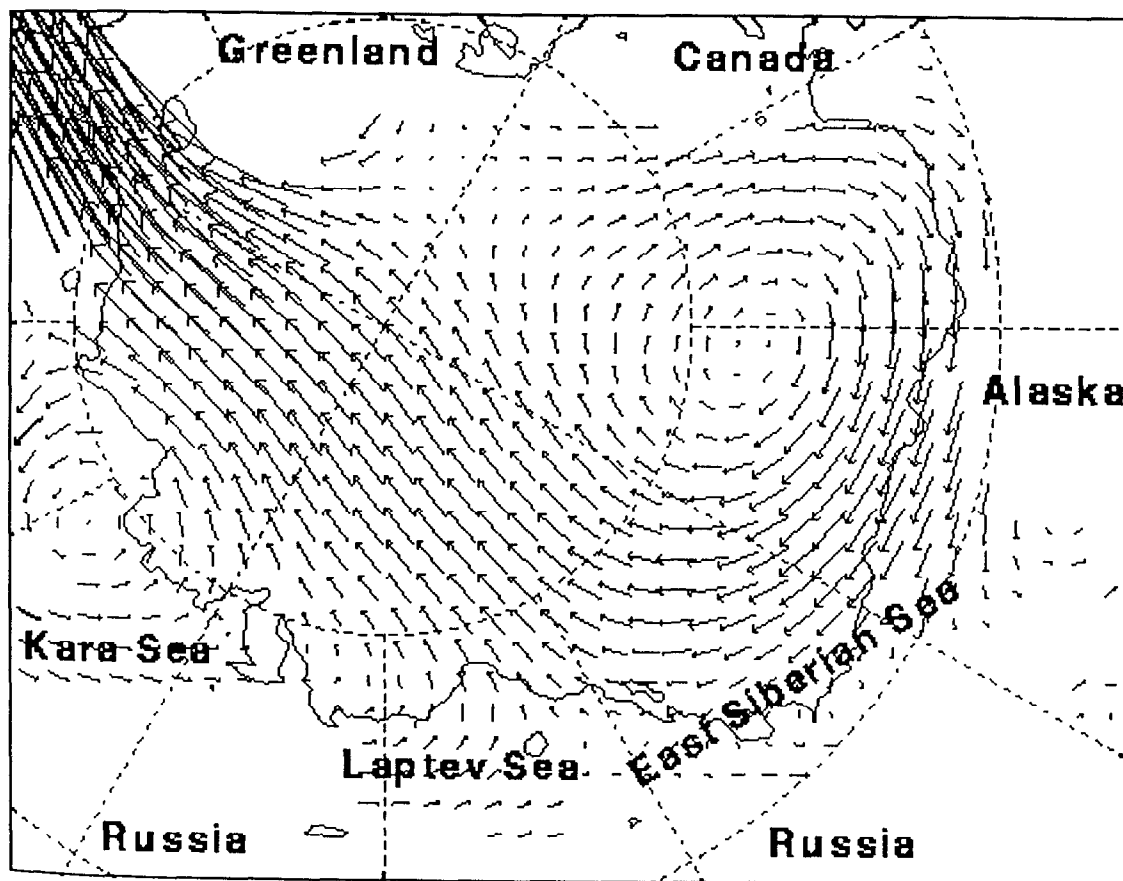


Figure 3-2. Mean field of ice motion in the Arctic Ocean for the years 1979 through 1994.

Comparing the annual flux of seawater from the Kara Sea ($3.8 \times 10^4 \text{ km}^3$) to the masses of sediment transported annually by seawater (1.3×10^8 tonnes) and ice (4×10^6 tonnes), the masses of sediment are minimal. The amounts of radionuclides transported by attachment to these masses of sediment will be correspondingly small. Should releases from nuclear wastes in the Kara Sea occur, the largest quantities of radionuclides will be exchanged by water transport to adjacent Arctic seas.

3.3 TRANSPORT SIMULATIONS: THE RAIG AND NIELSEN ET AL. (1995) COMPARTMENTAL MODELS

The transport simulations conducted as part of the ANWAP risk assessment are based on a compartmental transport model developed by the RAIG. The group also has implemented a modified version of a compartmental model developed by Nielsen et al. (1995) for assessing radionuclide transport in the Arctic Ocean in order to establish benchmarks with another assessment-level model. Below are descriptions of the basic attributes of the two models.

3.3.1 RAIG Compartmental Model

The compartmental model (CM) developed by the RAIG is a numerical formulation that simulates radionuclide transport by solving the basic system of coupled mass-balance equations, defined by Eq. 3-1, for multiple compartments throughout the Arctic Ocean. The RAIG CM has a compartmental structure consisting of boxes that represent the Arctic Ocean's major seas and the Bering Sea. Compartment volumes and depths were based on analyses of bathymetric data, while water exchanges were determined from simulations of ocean currents via a three-dimensional, coupled ocean-ice model (Cheng and Preller, 1996). The commercially available software package, STELLA II [High Performance Systems Inc., 45 Lyme Road, Hanover, NH, 03755], was used to solve the set of linked ordinary differential equations representing the various compartments. The modeling system developed is able to simulate instantaneous or time-varying releases of a radionuclides in a given source compartment, such as the Kara Sea.

Compartmental Configuration

The basic compartmental structure of the RAIG model was developed at a workshop in Sequim, Washington (Oct. 16–18, 1995), that dealt primarily with the use of various kinds of models to assess the impacts of nuclear wastes in the Arctic Ocean. Important objectives for developing the compartmental structure were to define compartments that (1) could be used to assess the transport of radionuclides from given sources (primarily nuclear wastes in the Kara Sea, and secondarily, the Northwest Pacific Ocean) to Alaskan waters and (2) reflect the major ocean basins and circulation patterns in the Arctic Ocean. The compartmental structure that emerged from the workshop covered sub-Arctic and Arctic waters from the Aleutian Islands and Bering Sea to the Norwegian and Greenland Seas. This extended domain was defined in order to provide a capability for assessing potential impacts over a wide region, although the focus was on Alaska. For example, the RAIG model includes several compartments along the north coast of the FSU from the Kara Sea to the Chukchi Sea to address a potential transport pathway from the Kara Sea to Alaskan waters. Compartments along the FSU and Alaskan Coasts include separate coastal and

shelf regions. The coastal regions are defined roughly as those waters extending outward from the coastline to a depth of 50 m. The shelf regions extend outward from this 50 m depth to the approximate location where the shelf drop-off begins. This includes water from 50 to 1,000 m deep. Four factors lead to extension of the model domain to the Aleutian Islands: (1) the migratory patterns of some of the marine mammals which extend to the Aleutians, (2) coastal populations south of the Arctic Circle, which are included in the assessment, (3) the Aleutians form a logical boundary between the North Pacific and the Bering Sea, and (4) it could accommodate the possibility of including a radionuclide release in the Northwest Pacific Ocean.

Figure 3-3 depicts the 21 compartmental regions, some of which are stacked two deep in the vertical direction. The boundary between vertical regions is approximately at the 500 m depth level. Exchanges occur between adjacent regions both in the horizontal and vertical direction. Radionuclide releases occur in the Kara Sea estuary, compartment 7, to represent inputs from the Ob and Yenisey rivers, and compartment 8 is used as the source compartment for releases from nuclear wastes in the Kara Sea, including bays along the coast of Novaya Zemlya. An additional release from the Northwest Pacific Ocean is treated as a boundary condition along the Southern Bering Sea/Aleutian boundary.

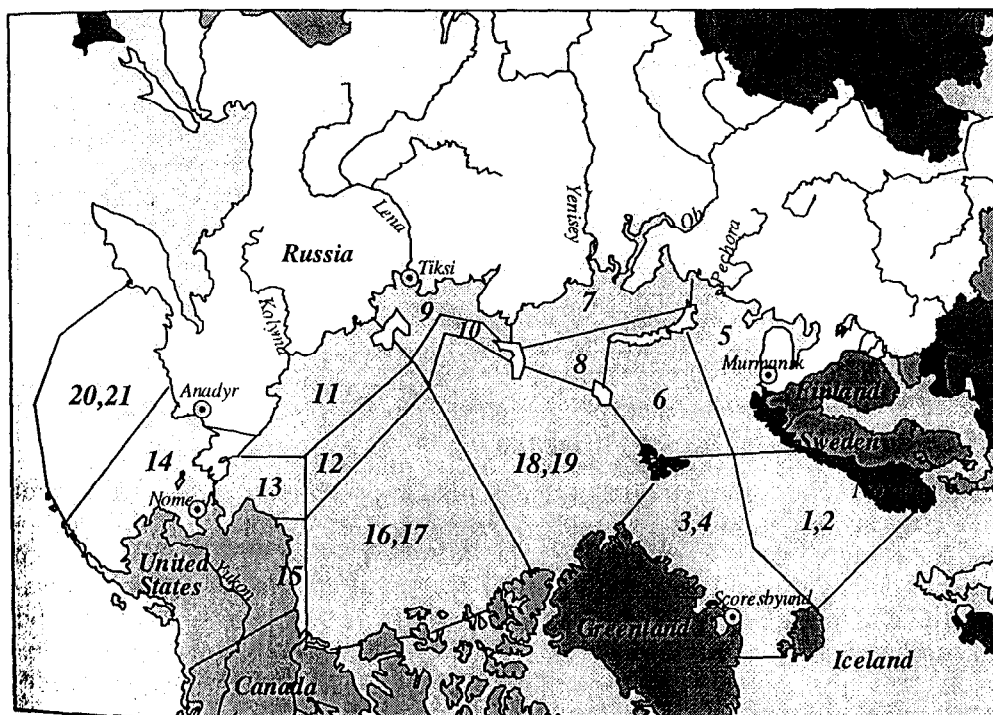


Figure 3-3. Locations of the water compartments used in the RAIG model. Two numbers designate areas that include two stacked boxes to represent a vertical section of the ocean: the first number represents the upper compartment, and the second one the lower compartment.

A diagram in Figure 3-4 shows the connectivity among the various compartments. This connectivity defines which compartments interact and influence the behavior of other compartments. Additional data describe the boundary conditions. These boundaries define the physical extent of the region considered for the Arctic risk assessment. It is across these boundaries that interaction to other ocean regions may occur and influence the results. In the RAIG model, interaction between the Arctic and Pacific oceans occurs at compartments 14, 20, and 21 in the Bering Sea. Interactions between the Arctic and Atlantic oceans occur at compartments 1 and 2 (the Norwegian Sea), 3 and 4 (the Greenland Sea), and 16 (adjacent to the Canadian archipelago).

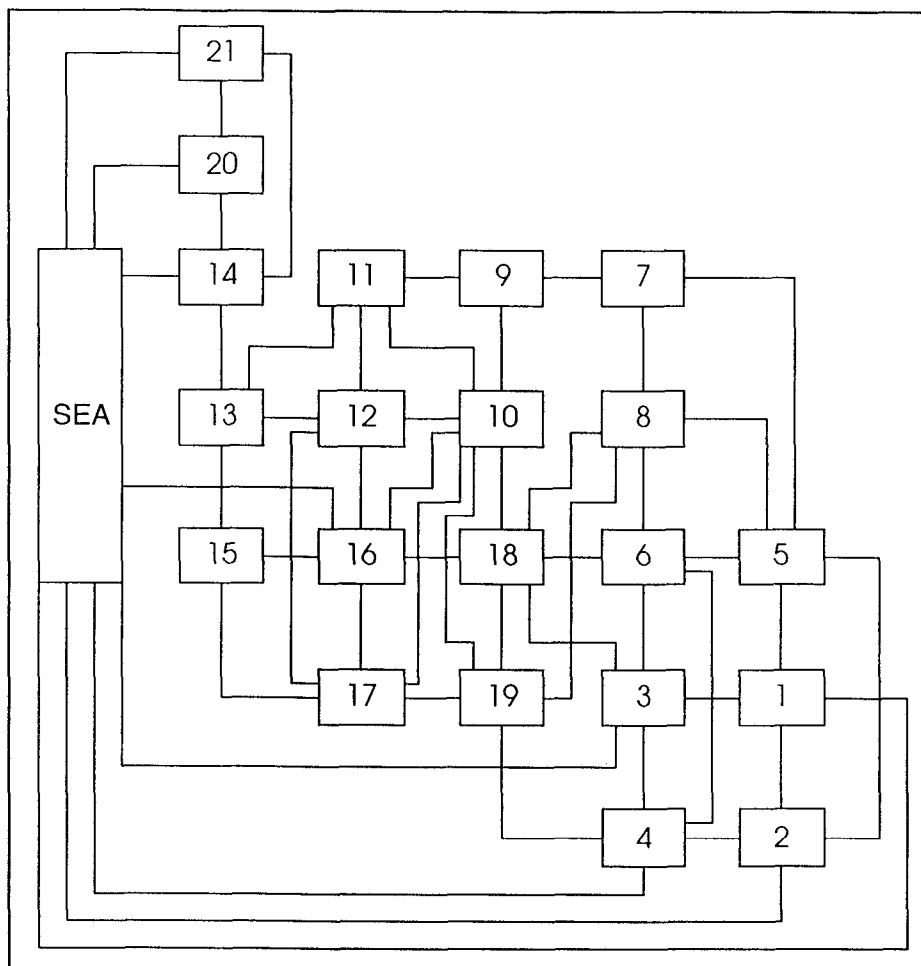


Figure 3-4. Water exchanges between ocean compartments in the RAIG model.

Parameterization of Compartmental Input Variables

The accurate characterization of water movements between boxes is perhaps the most important part of implementing a compartmental model. Usually, water flows are estimated from oceanographic data covering the waters being assessed (e.g., Evans, 1985). However, even with such data it can be difficult to quantify the water exchanges between several compartments. The water exchanges in the RAIG CM were determined by a methodology developed by Marietta and Simmons (1988), who used an ocean-circulation model (OCM) to determine the water flows between compartments. In their approach the researchers first run an OCM to determine the three-dimensional flow of water through the ocean region being assessed, and then process the results of that simulation to provide the water flows across the specific ocean compartments used to represent the assessment domain. Flows also can be adjusted, as appropriate, to reflect oceanographic data on various currents in the region being assessed. Nielsen et al. (1995) also adopted this approach for the development of a CM of the Arctic Ocean.

Once the compartmental structure of the RAIG model was defined, the next step in model implementation was to determine the volumes and depths of the compartments and the water exchange rates between compartments. The keys to determining the values of these parameters were a coupled ice-ocean computer model implemented by Cheng and Preller (1996) to determine the movement of water in the seas representing the assessment domain, and special soft-

ware for rapidly analyzing the input and output files of the ice-ocean circulation model to determine the inputs to the RAIG CM.

The coupled ice-ocean model used to simulate the movement of sea ice and ocean currents is based on the coupling of the Hibler ice model (Hibler, 1979, 1980) to the Cox (1984) ocean model. The equations used by both models are defined in spherical coordinates. The model grid has been transformed and rotated to avoid a numerical singularity at the grid point representing the North Pole. Cheng and Preller (1996) give a detailed description of the model equations written in spherical coordinates and the grid transformation. The model was originally designed to include all sea-ice-covered regions in the northern hemisphere and extends from the pole to approximately 30° N latitude. This domain includes those seas with a partial sea-ice cover such as the Sea of Okhotsk, Sea of Japan, and the Yellow Sea. It also includes the Labrador Sea, Hudson Bay, Baffin Bay, and the East Greenland and Barents seas on the Atlantic side. The horizontal grid resolution of the model is 0.28 degrees. The model uses fifteen levels to resolve the depth of the ocean. The first level is shallowest and extends to 30 m depth. The thickness of each level increases with depth. The ETOPO5 bathymetry data helps define the model geometry and bathymetry. Several channels and straits are artificially closed when this data is averaged onto the model grid (i.e., the channel connecting the Baltic to the North Sea). In addition, some islands, adjacent to deep trenches, are averaged in such a way that they become sea points. Several such problem areas have been edited manually and corrected. Manual editing to open several straits (i.e., the Kara Gate) also has resulted in artificially widening these straits. Many of the Aleutian and Kuril Islands had to be edited manually back into the model geometry.

The ice and ocean models are coupled by exchanging necessary heat and salinity flux as well as interfacial stress information. Two of the ocean-model equations that use daily ice-model information are the temperature and salinity equations. The temperature equation follows:

$$\frac{\partial T}{\partial t} + \nabla \cdot (\mathbf{u}T) = K_H \nabla^2 T + K_Z \frac{\partial^2 T}{\partial z^2} - \frac{f_A \delta(z) R_0 \theta(T - T_f)}{Z_{\text{mix}}} - R_t (T - T_0), \quad (3-11)$$

where

T	=	the water temperature,
\mathbf{u}	=	the ocean current,
K_H	=	coefficient of the horizontal eddy diffusion,
∇^2	=	horizontal Laplacian operator,
K_Z	=	coefficient of the vertical eddy diffusion,
f_A	=	ice growth/melting rate in open water from atmospheric forcing only,
$\delta(z)$	=	delta function, i.e., one in the mixed-layer and zero otherwise,
R_0	=	ratio of the latent heat of fusion of sea ice to the heat capacity of seawater,
$\theta(T - T_f)$	=	one when the mixed-layer temperature, T , is greater than the freezing point, T_f , and zero otherwise,
R_t	=	robust constraint for water temperature and salinity,
T_0	=	the Levitus monthly climatology temperature, and
Z_{mix}	=	the mixed-layer thickness.

The robust constraint, as defined by Sarmiento and Brian (1982), is set at 250 days. This is sufficient to keep the ocean temperature and salinity from dissipating because of eddy diffusion, but also allows the atmospheric heating and cooling effects to penetrate into the upper layer of the ocean model.

The salinity equation used in the ocean model is

$$\frac{\partial S}{\partial t} + \nabla \cdot (uS) = K_H \nabla^2 S + K_Z \frac{\partial^2 S}{\partial z^2} - \frac{0.035 S_f \delta(z)}{Z_{\text{mix}}} - R_t (S - S_0), \quad (3-12)$$

where

$$\begin{aligned} S &= \text{salinity,} \\ S_f &= \text{total ice growth rate in open water, and} \\ S_0 &= \text{the Levitus monthly climatology salinity.} \end{aligned}$$

A similar robust constraint is used in the salinity equation. The freezing temperature used in the model is dependent on the salinity as defined by the following equation:

$$T_f = -54.4 S, \quad (3-13)$$

where S is the salinity. The mixed layer oceanic heat fluxes are defined as the heat advected and diffused into each grid cell, and have the following forms:

$$-\nabla \cdot (uT), K_H \nabla^2 T, K_Z \frac{\partial^2 T}{\partial z^2}, \quad (3-14)$$

each multiplied by the water mass and its heat capacity. Vertical mixing and vertical heat convection in the Cox ocean model take place whenever large enough density differences develop. In the coupled model, the mixed-layer temperature depends on the open water condition. If the open water starts to grow sea ice, then the mixed-layer temperature is set at the freezing point. The open water does not grow sea ice if the atmospheric and oceanic heat fluxes are not cold enough. They simply reduce the mixed-layer temperature. In the melting seasons, these heat fluxes warm up the mixed-layer or melt the existing sea ice. In coupling the ice and ocean models, sea ice is treated as a boundary layer blocking direct heat and momentum exchanges between the atmosphere and ocean. Surface wind stress passes momentum to the sea ice, some of which moves the sea ice, while another part transfers into the internal ice. Sea-ice motion is applied as a stress to the top layer of the ocean.

A variable drag coefficient between sea ice and water was applied based on the boundary layer theory of McPhee (1990):

$$C_{diw} = \left(\frac{1}{k} \ln \left(\frac{h}{z_0} \right) \right)^{-2}, \quad (3-15)$$

where

C_{diw} is the coefficient,

- k = the von Karmon constant, 0.41;
- z_0 = the ice roughness (0.01 m); and
- h = the ice thickness, which is set to be greater than z_0 at all times.

When h is equal to 2.5 meters, the drag coefficient is equal to the constant value used by Hibler (1979), 0.0055. Note that the drag coefficient decreases as the ice thickness increases, i.e., there is very little drag stress on thick ice from water. On the other hand, the drag stress becomes the dominant factor over wind stress when h is small and very close to z_0 .

Numerical model experiments are run in the following way. In the coupled case, the model is initialized from a fall "model climatology" based on the model results using 1986 atmospheric forcing (i.e., wind-generated ocean currents) from the U.S. Navy's global atmospheric model, the Navy Operational Global Atmospheric Prediction System (NOGAPS). In the uncoupled case, the ocean model is "spun up" from Levitus climatology by running it for 5 years using a mean wind. In both cases, the model boundaries in the Atlantic and Pacific oceans are all treated as "closed" boundaries. The model calculation from which these transports were determined used the following parameters: horizontal eddy diffusion = 10^6 cm²/s, vertical eddy diffusion = 1 cm²/s, horizontal eddy viscosity = 10^8 cm²/s, and the vertical eddy viscosity = 1 cm²/s. The time step used in this model run was 1 hour for temperature and salinity and 6 minutes (0.1 hour) for the stream function and ocean currents (i.e., the distorted physics method of Bryan (1984)).

To expedite the process of converting the ocean-model results for the three-dimensional simulations to water exchange rates between compartments in the RAIG CM, the RAIG developed an automated process that divides the ocean into compartments, sums areas and volumes, and then computes water exchanges (implemented as a computer program, termed PFIG). The automated process allows an analyst to define arbitrary polygons within the Arctic Ocean and uses bathymetry data and water circulation predictions from the ocean circulation model to create the necessary transfer rates for the RAIG CM.

Table 3-2 shows the compartmental volumes and depths for the various compartments in the RAIG model obtained from the PFIG software. Table 3-3 presents water exchanges between the various compartments (based on the ocean-current predictions from the coupled ice-ocean model). The original water flux predicted by the ocean circulation model for the Bering Strait was considerably lower than the measured current of 0.89×10^6 m³/s (Roach et al., 1995). To compensate for this underprediction, the RAIG increased the flow of Pacific Ocean water from the Bering Sea to the Chukchi Sea to 1×10^6 m³/s, and routed this additional flow through adjacent compartments so that it exits the Arctic Ocean via the Canadian archipelago (see Table 3-3).

Table 3-2. Data on compartment volumes, depths, sediment loadings, and sediment deposition for the RAIG compartmental model.

Region	Box Id	Volume m ³	Depth m	Sediment Load t/m ³	Sedimentation Rate t/m ² -y
Norwegian Sea, upper	1	5.0×10^{14}	4.6×10^2	1×10^{-6}	1×10^{-4}
Norwegian Sea, lower	2	1.9×10^{15}	1.7×10^3	1×10^{-6}	2×10^{-5}
Greenland Sea, upper	3	4.8×10^{14}	4.3×10^2	1×10^{-6}	1×10^{-4}
Greenland Sea, lower	4	1.5×10^{15}	1.4×10^3	1×10^{-6}	2×10^{-5}
Barents Sea, South	5	1.3×10^{14}	2.3×10^2	6×10^{-6}	1×10^{-3}
Barents Sea, North	6	2.3×10^{14}	2.8×10^2	6×10^{-6}	5×10^{-4}
Kara Sea, estuary	7	2.9×10^{13}	7.3×10^1	3×10^{-6}	1×10^{-3}
Kara Sea	8	1.0×10^{14}	2.7×10^2	6×10^{-6}	3×10^{-4}
Laptev Sea, coastal	9	2.4×10^{13}	5.1×10^1	3×10^{-6}	1×10^{-3}
Laptev Sea, shelf	10	1.6×10^{14}	9.7×10^2	1×10^{-6}	1×10^{-4}
East Siberian Sea, coastal	11	4.4×10^{13}	6.0×10^1	3×10^{-6}	1×10^{-3}
East Siberian Sea, shelf	12	2.6×10^{14}	6.4×10^2	1×10^{-6}	1×10^{-4}
Chukchi Sea	13	2.3×10^{13}	7.3×10^1	3×10^{-6}	1×10^{-3}
Bering Sea, North	14	6.7×10^{13}	9.8×10^1	3×10^{-6}	1×10^{-3}
Beaufort Sea	15	7.7×10^{13}	6.6×10^2	1×10^{-6}	1×10^{-4}
Amerasian Basin, upper	16	1.3×10^{15}	4.6×10^2	1×10^{-6}	1×10^{-4}
Amerasian Basin, lower	17	5.6×10^{15}	2.0×10^3	1×10^{-6}	2×10^{-5}
Eurasian Basin, upper	18	1.0×10^{15}	4.8×10^2	1×10^{-6}	1×10^{-4}
Eurasian Basin, lower	19	5.6×10^{15}	2.6×10^3	1×10^{-6}	2×10^{-5}
Bering Sea South, upper	20	5.5×10^{14}	4.8×10^2	1×10^{-6}	1×10^{-4}
Bering Sea South, lower	21	3.0×10^{15}	2.6×10^3	1×10^{-6}	2×10^{-5}
Sea	22	1.0×10^{18}	3.4×10^3	1×10^{-6}	2×10^{-5}

The combination of compartmental volume and related exchange rates between compartments are the inputs required to calculate rate constants (Eq. 3-2) for simulating the transfer of radionuclides between compartments. The depth of a compartment, the mass loading of particulate matter, the sedimentation rate, and K_d of a radionuclide are required to determine the rate constants for particle scavenging (Eq. 3-3). For the transport simulations, the RAIG used a K_d of 100 m³/kg for both ²⁴¹Am and ²³⁹Pu, as there was insufficient data to distinguish between the values summarized in Table 3-1 for these two radionuclides. The K_d s presented in Table 3-1 for ¹³⁷Cs and ⁹⁰Sr were considerably smaller than those for ²⁴¹Am and ²³⁹Pu. The RAIG selected values of 0.1 and 0.004 m³/kg to represent ¹³⁷Cs and ⁹⁰Sr. These values constitute reasonable and conservative lower bounds, which means that most of the radioactivity for these two nuclides would be associated with the dissolved phase.

Table 3-3. Volumetric exchanges of water between compartments of the RAIG compartmental model. Values have been rounded to two significant figures.

From box	To box	Flux ($\text{km}^3 \text{ y}^{-1}$)	From box	To box	Flux ($\text{km}^3 \text{ y}^{-1}$)	From box	To box	Flux ($\text{km}^3 \text{ y}^{-1}$)
Sea	1	2.4×10^5	9	10	3.7×10^4	19	17	3.9×10^5
Sea	2	6.8×10^4	10	9	2.4×10^4	19	18	3.6×10^4
Sea	3	2.7×10^4	10	12	5.2×10^3	20	Sea	2.8×10^5
Sea	4	2.0×10^2	10	16	4.9×10^3	20	14	1.2×10^5
Sea	14	2.0×10^2	10	17	4.8×10^3	20	21	3.3×10^4
Sea	16	5.1×10^3	10	18	8.1×10^4	21	Sea	3.3×10^5
Sea	20	3.4×10^5	10	19	8.9×10^4	21	14	1.6×10^3
Sea	21	3.0×10^5	11	9	1.4×10^4	21	20	6.2×10^3
1	Sea	5.3×10^4	11	10	1.5×10^3			
1	2	5.6×10^4	11	12	3.8×10^4			
1	3	2.3×10^5	11	13	1.0×10^3			
1	5	8.5×10^4	12	10	5.6×10^3			
2	Sea	1.3×10^5	12	11	3.8×10^4			
2	1	5.5×10^4	12	13	3.3×10^3			
2	4	1.1×10^5	12	16	1.5×10^5			
2	5	1.5×10^3	12	17	4.3×10^4			
3	Sea	1.4×10^5	13	11	1.6×10^4			
3	1	1.2×10^5	13	12	4.2×10^4			
3	4	6.8×10^4	13	14	4.0×10^2			
3	6	3.9×10^3	14	Sea	1.0×10^2			
3	18	9.1×10^4	14	13	3.2×10^4			
4	Sea	1.6×10^4	14	20	8.5×10^4			
4	2	1.6×10^5	14	21	2.4×10^3			
4	3	2.1×10^4	15	13	2.3×10^4			
4	19	3.9×10^4	15	16	4.3×10^4			
5	1	6.8×10^3	15	17	4.6×10^4			
5	2	2.1×10^3	16	Sea	3.6×10^4			
5	6	1.8×10^5	16	10	1.0×10^2			
5	7	8.0×10^2	16	12	1.1×10^5			
5	8	1.0×10^3	16	15	5.6×10^4			
6	3	7.6×10^4	16	17	3.6×10^4			
6	4	4.8×10^3	16	18	1.2×10^5			
6	5	9.8×10^4	17	12	4.4×10^4			
6	8	2.7×10^4	17	15	5.5×10^4			
6	18	1.5×10^3	17	16	6.0×10^4			
7	5	8.0×10^2	17	19	3.6×10^5			
7	8	1.8×10^4	18	3	7.2×10^4			
7	9	9.0×10^2	18	6	2.0×10^4			
8	5	4.0×10^2	18	8	9.4×10^3			
8	6	9.2×10^3	18	10	7.7×10^4			
8	7	1.8×10^4	18	16	9.2×10^4			
8	18	2.4×10^4	18	19	7.9×10^4			
8	19	4.2×10^3	19	4	5.9×10^4			
9	7	9.0×10^2	19	10	8.7×10^4			

3.3.2 Compartmental Model of Nielsen et al. (1995)

Nielsen et al. (1995) developed a multi-compartment model to simulate the movement of radionuclides released into the Arctic seas from dumpsites in the Kara Sea. The basic mass-balance equations for simulating radionuclide transport are similar to ones used in the RAIG model. The model developed by Nielsen et al. (1995) includes compartments that encompass all of the world's oceans. Water flows between compartments are calculated using a three-dimensional ocean circulation model (Chartier, 1993). Figure 3-5 depicts the spatial arrangement of the surface or upper compartments for the Arctic Ocean, which represent generally the Arctic seas that form the Arctic Ocean. The most notable difference in the compartmental configuration of the RAIG model is that it includes a more refined treatment of the shelf areas along the Russian coastline, more compartments representing the Bering Sea adjacent to Alaska, and larger compartments for the central portion of the Arctic Ocean.

Because the primary focus of the RAIG is assessing the impacts that radionuclide releases could have on Alaskan waters, the team has implemented a modified version of the Nielsen et al. model that retains the compartmental structure shown in Figure 3-5, but consolidates the compartments representing the Atlantic Ocean and related seas into a single ocean compartment (denoted AORS) that is connected to the other world oceans (compartment 59). Recirculation to the Arctic Ocean occurs via transport through the Atlantic Ocean and related seas, the other world oceans, and then the Bering Strait. The modified compartmental configuration is shown in Figure 3-6. The

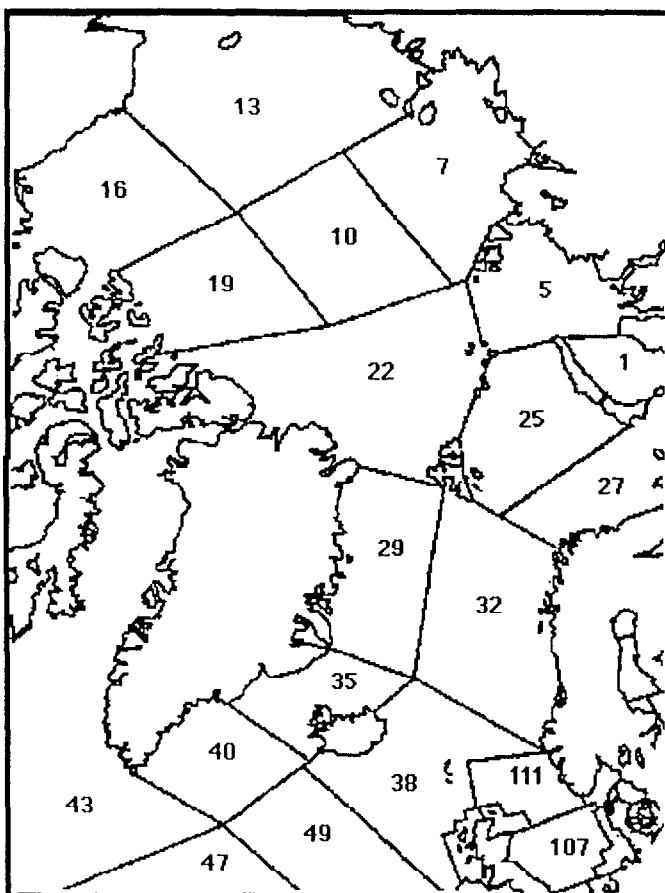


Figure 3-5. Locations of the surface-ocean compartments used in the Nielsen et al. (1995) model.

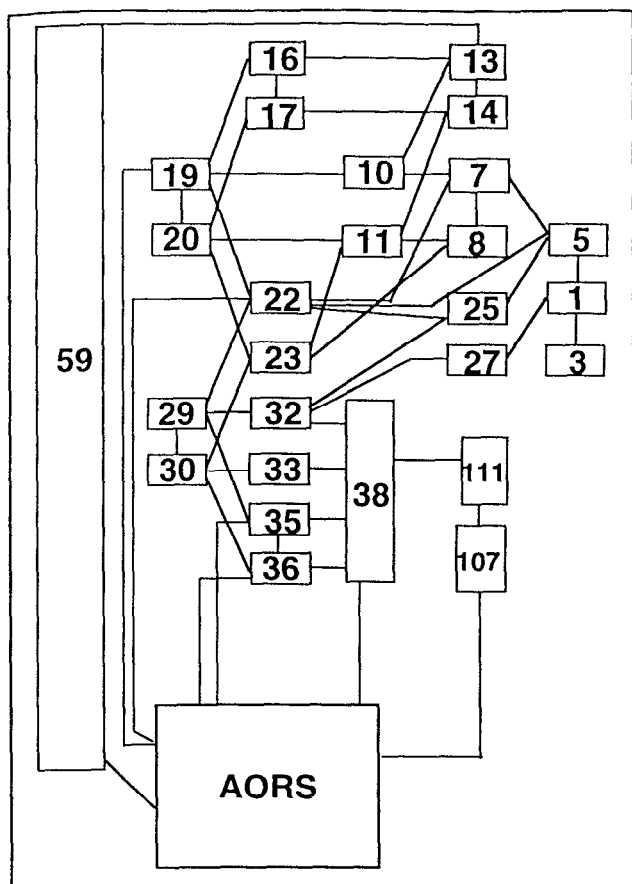


Figure 3-6. Modification of the compartmental structure used in Nielsen et al. (1995). The principal change is the consolidation of compartments representing the Atlantic Ocean and related seas into one compartment, denoted AORS.

RAIG also has assumed that particle resuspension over the assessment domain is far less important than particle scavenging, and therefore treats sediments as a sink or reservoir, with no transfers via pore-water diffusion or resuspension to overlying water columns. Table 3-4 presents the compartmental volumes, sediment loadings, and sedimentation rates used for each compartment. Volumetric exchanges between compartments are given in Table 3-5.

3.3.3 Model Intercomparisons and Sensitivities

To explore some of the uncertainties associated with the various source terms as well as the transport models, the RAIG will use the two CMs to simulate the alternative release scenarios. Both models were implemented in STELLA II. The simulations presented in this report were obtained using the 4th order Runge-Kutta option with a fixed time step of 0.1 year. In order to gain confidence that the STELLA II software was being used properly, the governing equations were also solved numerically using an ordinary differential equation solver with an adaptive time step. The adaptive method allows the time step to be increased or decreased according to the numerical behavior of the solution, thus allowing for an efficient use of the computer resource. It was determined that the two methods give essentially identical results for a step size of 0.1 year.

Tables 3-6 and 3-7 present simulations of 1 TBq instantaneous releases of ^{241}Am , ^{137}Cs , and ^{239}Pu to the Kara Sea and the Kara Sea estuary using the RAIG and modified Nielsen et al. models. For these particular simulations the RAIG used the IAEA-recommended K_d s for the three nuclides in

both models (IAEA, 1995). The simulations of ^{137}Cs transport by the two models result in predicted concentrations for the Beaufort and Chukchi Seas that are quite comparable (concentrations are within a factor of 3).

Table 3-4. Data on compartment volumes, depths, sediment loadings, and sediment deposition for the modified Nielsen et al. (1995) compartmental model.

Region	Box Id	Volume m^3	Depth m	SSL t/m^3	SR $\text{t}/\text{m}^2\text{-y}$
Western Kara Sea	1	1.2×10^{13}	7.0×10^1	3×10^{-6}	1×10^{-3}
Western Kara Sea deep	3	1.6×10^{13}	2.5×10^2	6×10^{-6}	3×10^{-4}
Eastern Kara Sea	5	7.0×10^{13}	7.0×10^1	3×10^{-6}	1×10^{-3}
Laptev Sea, upper	7	2.2×10^{14}	3.3×10^2	1×10^{-6}	1×10^{-4}
Laptev Sea, lower	8	4.8×10^{14}	7.0×10^2	1×10^{-6}	2×10^{-5}
Eurasian Basin, upper	10	2.7×10^{14}	3.3×10^2	1×10^{-6}	1×10^{-4}
Eurasian Basin, lower	11	2.7×10^{15}	3.2×10^3	1×10^{-6}	2×10^{-5}
East Siberian Sea, upper	13	3.6×10^{14}	3.3×10^2	1×10^{-6}	1×10^{-4}
East Siberian Sea, lower	14	9.9×10^{14}	9.0×10^2	1×10^{-6}	2×10^{-5}
Beaufort Sea, upper	16	2.6×10^{14}	3.3×10^2	1×10^{-6}	1×10^{-4}
Beaufort Sea, lower	17	8.8×10^{14}	1.2×10^3	1×10^{-6}	2×10^{-5}
Canadian Arctic Sea, upper	19	2.1×10^{14}	3.3×10^2	1×10^{-6}	1×10^{-4}
Canadian Arctic Sea, lower	20	2.1×10^{14}	2.2×10^3	1×10^{-6}	2×10^{-5}
Makarov and Fram Basin, upper	22	4.7×10^{14}	3.3×10^2	1×10^{-6}	1×10^{-4}
Makarov and Fram Basins, lower	23	4.1×10^{15}	2.9×10^3	1×10^{-6}	2×10^{-5}
Barents Sea North	25	1.6×10^{14}	2.0×10^2	6×10^{-6}	5×10^{-4}
Barents Sea South	27	1.6×10^{14}	2.0×10^2	6×10^{-6}	1×10^{-3}
Greenland Sea, upper	29	2.5×10^{14}	3.3×10^2	1×10^{-6}	1×10^{-4}
Greenland Sea, lower	30	1.4×10^{15}	1.8×10^3	1×10^{-6}	2×10^{-5}
Norwegian Sea, upper	32	2.9×10^{14}	3.3×10^2	1×10^{-6}	1×10^{-4}
Norwegian Sea, lower	33	1.7×10^{15}	1.9×10^2	1×10^{-6}	2×10^{-5}
Denmark Strait, upper	35	1.3×10^{14}	3.3×10^2	1×10^{-6}	1×10^{-4}
Denmark Strait, lower	36	8.0×10^{13}	2.0×10^2	1×10^{-6}	2×10^{-5}
Faroe Channel	38	1.9×10^{15}	1.4×10^3	1×10^{-6}	1×10^{-4}
North Sea Channel and North Sea North	111 and 107	1.1×10^{14}	1.0×10^2	6×10^{-6}	1×10^{-4}
Atlantic Ocean and related seas	AORS	1.5×10^{17}	3.8×10^3	1×10^{-6}	2×10^{-5}
Other world oceans	59	1.1×10^{18}	3.8×10^3	1×10^{-6}	2×10^{-5}

The largest differences between the models are for the predicted levels of ^{241}Am and ^{239}Pu in the two seas after an instantaneous release to the Kara Sea. Both of these nuclides are more particle reactive than ^{137}Cs , and consequently they are more effectively scavenged from the water column. The Kara Sea compartment of the modified Nielsen et al. model (see Figure 3-5) does not discharge directly to the central Arctic Ocean, as does the RAIG model, and therefore there is likely to be more depletion by particle scavenging in the coastal compartments (1 and 5).

Table 3-5. Volumetric exchange of water between compartments of the modified Nielsen et al. (1995) compartmental model. Note that some exchanges do not balance because of roundoff error.

From Box	To Box	Flux ($\text{km}^3 \text{ y}^{-1}$)	From Box	To Box	Flux ($\text{km}^3 \text{ y}^{-1}$)	From Box	To Box	Flux ($\text{km}^3 \text{ y}^{-1}$)
1	3	3.2×10^3	20	23	8.0×10^4	35	AORS	1.6×10^5
1	5	9.5×10^2	22	7	6.5×10^4	36	35	2.8×10^4
1	27	9.5×10^2	22	10	4.7×10^4	36	38	2.8×10^4
3	1	3.2×10^3	22	19	2.5×10^4	36	AORS	4.5×10^5
5	1	9.5×10^2	22	23	3.2×10^4	38	32	3.0×10^5
5	7	8.5×10^3	22	25	1.6×10^4	38	33	1.5×10^5
5	22	5.2×10^4	22	29	9.1×10^4	38	35	2.3×10^4
5	25	9.5×10^3	22	43	1.4×10^4	38	36	1.5×10^5
7	8	3.7×10^4	23	8	6.0×10^4	38	AORS	2.1×10^5
7	10	6.9×10^4	23	11	6.9×10^4	38	AORS	2.6×10^5
7	22	1.8×10^4	23	20	4.0×10^4	38	61	8.3×10^3
8	7	2.1×10^4	23	22	4.6×10^4	38	111/107	3.4×10^4
8	11	1.3×10^5	23	30	1.2×10^4	40	35	1.7×10^5
10	7	2.9×10^4	25	5	6.9×10^4	40	38	1.4×10^5
10	11	3.3×10^4	25	22	8.5×10^3	59	13	2.8×10^4
10	13	2.8×10^3	25	27	9.5×10^3	59	AORS	1.6×10^6
10	19	1.6×10^5	25	32	1.9×10^4	111/107	38	5.0×10^4
10	22	1.0×10^5	27	1	9.5×10^2	AOR	59	1.7×10^6
11	8	5.5×10^4	27	25	7.7×10^4			
11	10	2.2×10^4	27	32	3.2×10^4			
11	20	8.8×10^4	29	22	4.7×10^4			
11	23	1.1×10^5	29	30	9.2×10^4			
13	10	1.9×10^5	29	32	2.0×10^4			
13	14	1.4×10^5	29	35	1.9×10^5			
14	11	4.6×10^4	30	23	2.2×10^3			
14	13	1.4×10^5	30	29	3.0×10^4			
16	13	1.5×10^5	30	33	6.1×10^4			
16	17	4.5×10^4	30	36	1.4×10^5			
16	19	4.7×10^3	32	25	4.4×10^3			
17	14	4.7×10^4	32	27	9.9×10^4			
17	16	5.6×10^4	32	29	2.3×10^5			
17	20	1.5×10^4	32	33	7.4×10^4			
19	16	1.5×10^5	32	38	6.3×10^3			
19	20	3.2×10^4	33	30	1.3×10^5			
19	22	1.8×10^4	33	32	4.6×10^4			
19	43	1.4×10^4	33	38	1.1×10^5			
20	17	7.4×10^4	35	36	1.9×10^5			
20	19	2.2×10^4	35	38	7.4×10^4			

Table 3-6. Predicted concentrations of ^{241}Am , ^{137}Cs , and ^{239}Pu in the Beaufort and Chukchi seas after an instantaneous release of 1 TBq of each radionuclide in the Kara Sea.

Model	Location	Time After Release, y	Radionuclide		
			^{241}Am	^{137}Cs Concentration, Bq/m ³	^{239}Pu
RAIG	Beaufort Sea	10	1.4×10^{-5}	3.1×10^{-5}	2.7×10^{-5}
		100	3.5×10^{-6}	2.1×10^{-6}	9.8×10^{-6}
	Chukchi Sea	10	2.3×10^{-6}	1.4×10^{-5}	8.3×10^{-6}
		100	5.8×10^{-7}	9.4×10^{-7}	3.0×10^{-6}
Modified Nielsen et al.	Beaufort Sea	10	9.8×10^{-8}	6.9×10^{-5}	2.2×10^{-6}
		100	2.5×10^{-8}	2.0×10^{-6}	2.7×10^{-7}
	Chukchi Sea	10	6.5×10^{-8}	8.5×10^{-6}	1.2×10^{-6}
		100	2.6×10^{-8}	1.8×10^{-6}	2.1×10^{-7}

The result is accentuated for ^{241}Am because the IAEA K_d used in the simulation is a factor of 10 greater than the one for ^{239}Pu and hence there is more particle scavenging for this nuclide. To further explore the importance of particle scavenging in the concentrations predicted by the RAIG model, the RAIG ran two cases using ^{239}Pu , one with a K_d of 100 m³/kg (or 10⁵ unitless) and the other with its K_d set equal to zero. Without particle scavenging (i.e., $K_d = 0$ and the contaminant is completely in the water phase, with no sorption to suspended particles), the predicted concentrations in the Beaufort and Chukchi Seas after an instantaneous release in the Kara Sea were factors of 2 and 3 greater than with particle scavenging.

Table 3-7. Predicted concentrations of ^{241}Am , ^{137}Cs , and ^{239}Pu in the Beaufort and Chukchi seas after an instantaneous discharge of 1 TBq of each radionuclide to the Kara Sea estuary from the Ob or Yenisey rivers.

Model	Location	Time After Release, y	Radionuclide		
			^{241}Am	^{137}Cs Concentration, Bq/m ³	^{239}Pu
RAIG	Beaufort Sea	10	1.9×10^{-6}	2.6×10^{-5}	9.9×10^{-6}
		100	4.9×10^{-7}	2.0×10^{-6}	3.7×10^{-6}
	Chukchi Sea	10	3.2×10^{-7}	1.2×10^{-5}	3.1×10^{-6}
		100	8.1×10^{-8}	8.9×10^{-7}	1.2×10^{-6}
Modified Nielsen et al.	Beaufort Sea	10	1.2×10^{-6}	6.4×10^{-5}	1.2×10^{-5}
		100	3.4×10^{-7}	2.2×10^{-6}	2.8×10^{-6}
	Chukchi Sea	10	1.0×10^{-6}	3.5×10^{-5}	8.2×10^{-6}
		100	3.5×10^{-7}	1.9×10^{-6}	2.6×10^{-6}

The primary differences between the two compartmental models that account for differences in the predicted concentrations of the radionuclide contaminants are the arrangement of the compartments and the flows of water between the compartments. As a first-order comparison of water flows, Table 3-8 presents the Arctic Ocean water balances associated with the RAIG and modified Nielsen et al. models as well as those based on current measurements and oceanographic tracers. The RAIG model results fall between the water exchange rates for the Nielsen et al. model and those based on oceanographic measurements.

Table 3-8. Comparison of water exchange rates for the Arctic Ocean.

Exchange Point	Water Transport rates $\times 10^6 \text{ m}^3/\text{s}$		
	Estimated ^a	Source RAIG Model	Nielsen et al. (1995)
Bering Strait	1	1 ^b	0.89
Canadian Arctic Archipelago	-(2 to 2.1)	-1 ^b	-0.89
East Greenland Current	-7.1	-11	-14
West Spitsbergen Current	7.2	11	14

^a Water transport values are based on Schlosser et al. (1995), Aagaard and Greisman (1995), and Roach et al. (1995). Positive values represent flows into the Arctic Ocean, while negative values represent flows out of the Arctic Ocean.

^b These transport values were based on estimates available in the literature, as the coupled ice/ocean circulation model substantially under predicted these water exchanges.

3.3.4 Simulations of Radionuclide Release Scenarios

The three sources of nuclear wastes this assessment addresses (i.e., the Kara Sea dumpsites, riverine releases from inland waste sites, and nuclear materials in the Northwest Pacific Ocean) have different inventories of the principal radionuclides and different release mechanisms. To bracket the range of potential releases, the RAIG will predict concentrations associated with the instantaneous release of the total estimated inventories presented in Section 2 as well as time-varying releases resulting from the leaching of radionuclides from waste matrices. An instantaneous release case is clearly a worst-case scenario for the Kara Sea dumpsites, as it is difficult to postulate a mechanism by which the radionuclides would suddenly be transferred from waste to water. A more likely release mechanism is the slow discharge to water via corrosion and degradation of waste materials containing the radioactive substances. Riverine releases, on the other hand, could very well be simulated as an instantaneous or pulse-type release, because one postulated release mechanism is retention dams' failure to hold back radioactive liquid wastes adjacent to tributaries of the Ob and Yenisey rivers.

Releases to the Kara Sea

Instantaneous Releases

To facilitate comparisons of the release scenarios, the RAIG simulates the discharge of 1 TBq (10^{12} Bq) of each of the radionuclides to the Kara Sea. For comparison, the estimated inventories as of 1994 (see Section 2) were 8.3, 6.2, 950, and 1,000 TBq for ^{241}Am , ^{239}Pu , ^{90}Sr , and ^{137}Cs , respectively. Figure 3-7 depicts the time-varying concentration of ^{137}Cs in the Chukchi, Beaufort, and Bering Seas resulting from the release of 1 TBq ($K_d = 0.3 \text{ m}^3/\text{kg}$). The Beaufort Sea attains a higher peak concentration than the Chukchi Sea (about a factor of 2 higher), but both compartments reach the peak in about 11 to 12 years. Similar results were obtained for ^{90}Sr , as both Cs and Sr behave almost identically (that is, as a conservative solute) for the K_d s presented in Table 3-1. The peak concentration for ^{137}Cs of about $3 \times 10^{-5} \text{ Bq/m}^3$ must be multiplied by 1,000 to obtain the estimated concentration associated with a release of the total inventory as of 1994, or 0.03 Bq/m^3 .

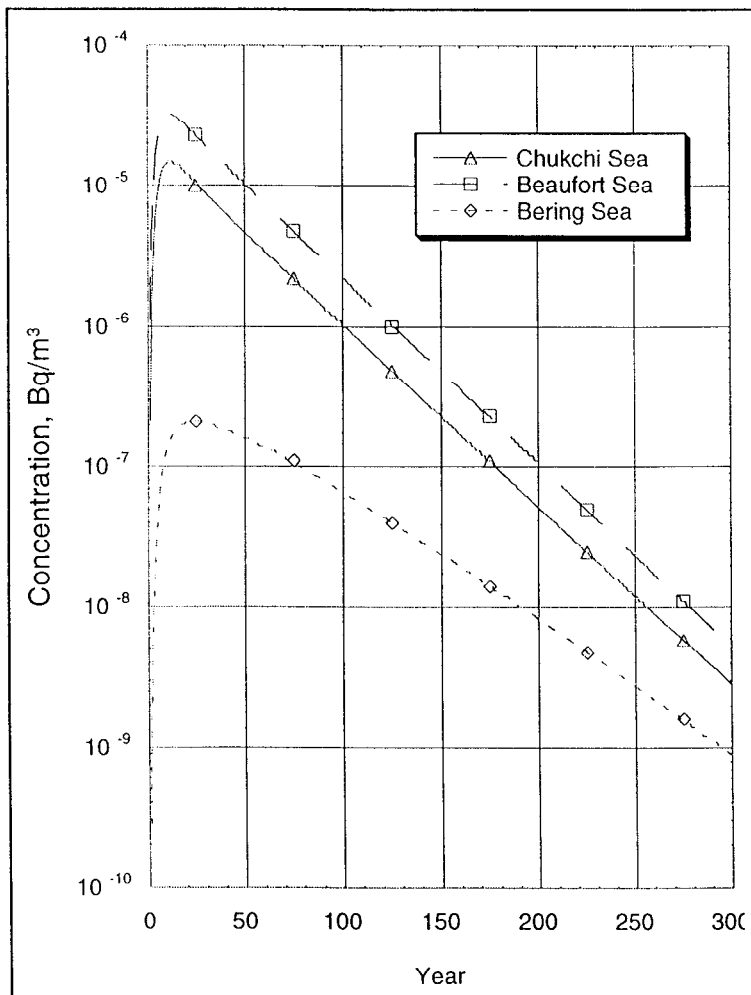


Figure 3-7. Concentrations of ^{137}Cs in the Chukchi, Beaufort, and Bering seas resulting from an instantaneous release of 1 TBq in the Kara Sea.

Time-Varying Releases

Figures 3-8, 3-9, and 3-10 present the Chukchi, Beaufort, and Bering seas' four radionuclide concentrations resulting from the time-varying nuclide releases into the Kara Sea from the wastes dumped there (Figure 2-7 shows the release-rate changes as a function of time.) Initial releases begin in the year 2000 and peak about 50 years later. A secondary peak occurs around 2300 as a result of the failure of containers holding SNFs. The highest fission-products concentrations in the Beaufort and Chukchi seas occur in 2080; the highest in the Bering Sea occur about 20 years later because of the transport time lag. Actinide concentrations are highest after the waste containers fail. Table 3-9 presents the times at which the peak doses occur and the associated concentrations of the four nuclides at that time. Because the dose is dominated by ^{137}Cs , the peak doses do not coincide with the times of the highest predicted actinide concentrations.

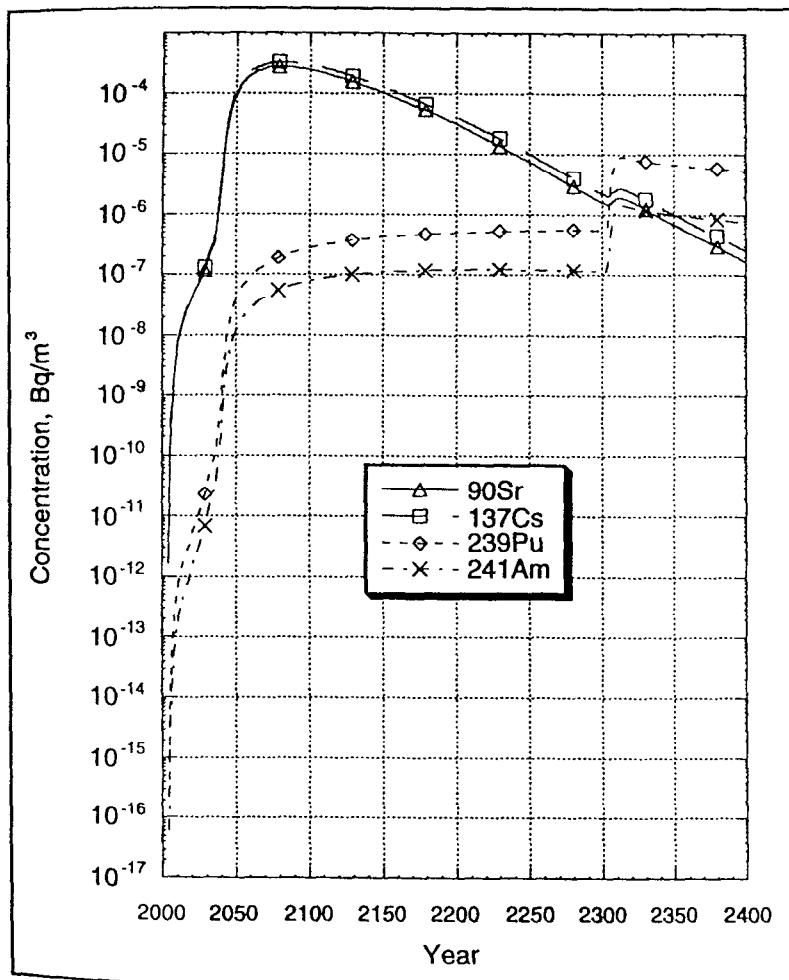


Figure 3-8. Concentrations of ^{241}Am , ^{137}Cs , ^{239}Pu , and ^{90}Sr in the Chukchi Sea resulting from the time-varying release of radionuclides from the Kara Sea nuclear wastes.

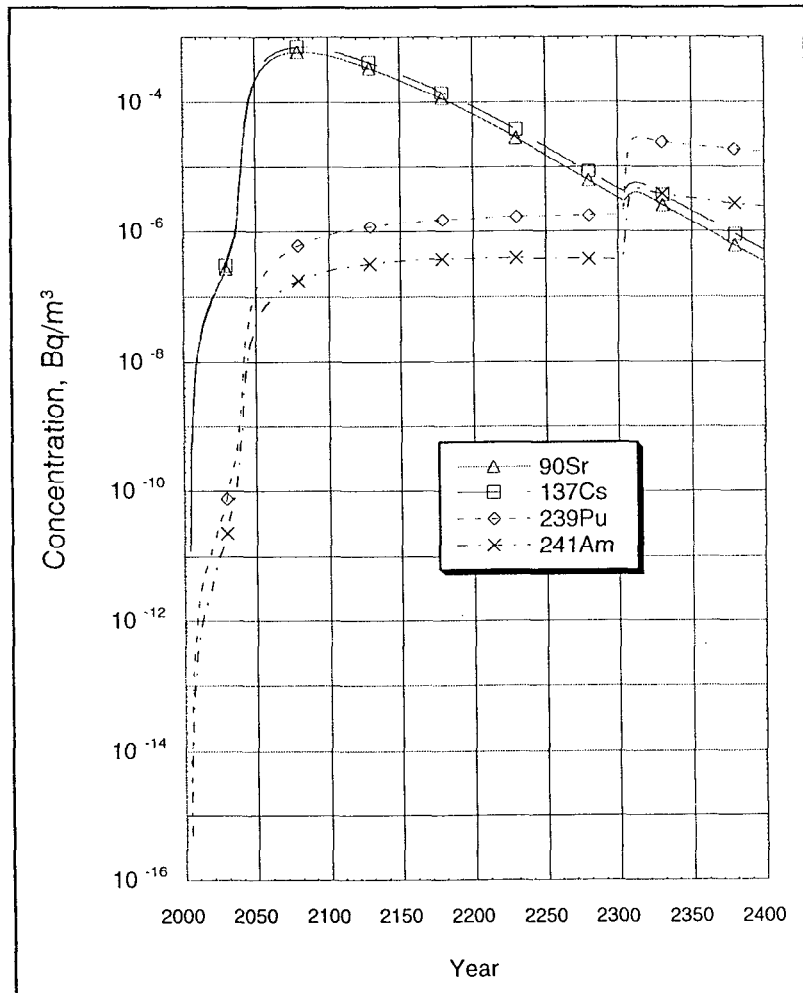


Figure 3-9. Concentrations of ²⁴¹Am, ¹³⁷Cs, ²³⁹Pu, and ⁹⁰Sr in the Beaufort Sea resulting from the time-varying release of radionuclides from the Kara Sea nuclear wastes.

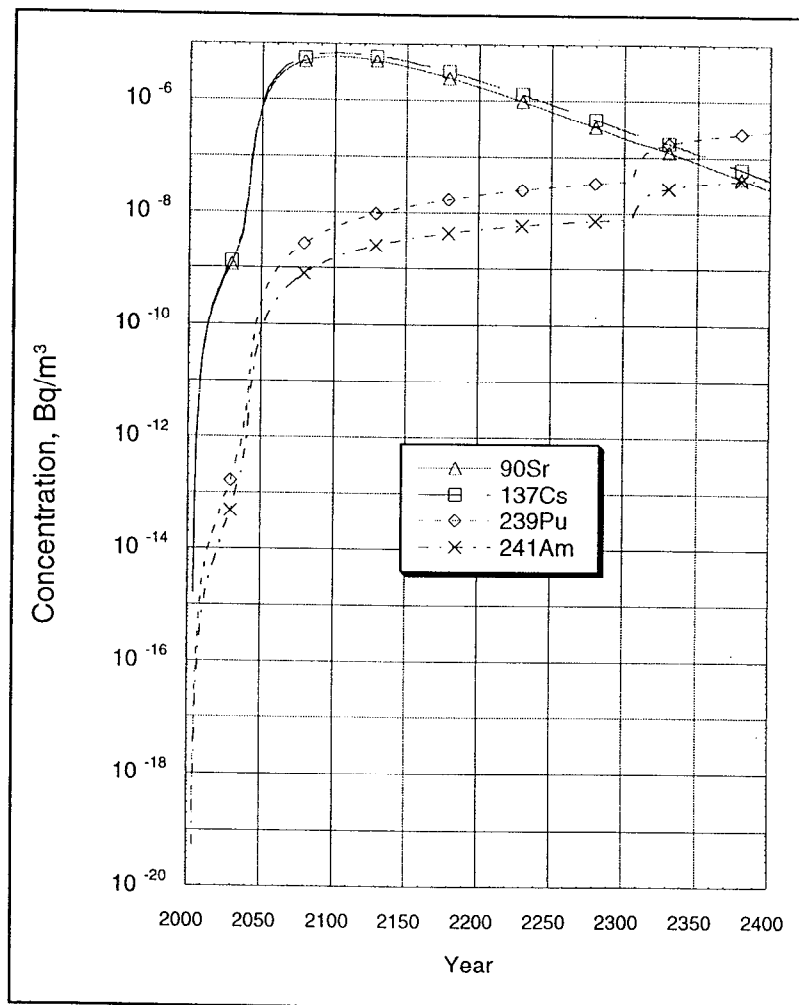


Figure 3-10. Concentrations of ²⁴¹Am, ¹³⁷Cs, ²³⁹Pu, and ⁹⁰Sr in the Bering Sea resulting from the time-varying release of radionuclides from the Kara Sea nuclear wastes.

Table 3-9. Concentrations associated with peak doses resulting from different source-term scenarios.

Scenario/Location	Time of Peak Dose ^a	Radionuclide			
		²⁴¹ Am	¹³⁷ Cs	²³⁹ Pu	⁹⁰ Sr
		Concentration, Bq/m ³			
Instantaneous release to the Kara Sea					
Beaufort Sea	12	2.2 × 10 ⁻⁴	3.2 × 10 ⁻²	1.6 × 10 ⁻⁴	3.0 × 10 ⁻²
Bering Sea	25	9.5 × 10 ⁻⁷	2.1 × 10 ⁻⁴	7.4 × 10 ⁻⁷	2.0 × 10 ⁻⁴
Chukchi Sea	12	6.8 × 10 ⁻⁵	1.5 × 10 ⁻²	5.2 × 10 ⁻⁵	1.4 × 10 ⁻²
Time-varying release to the Kara Sea					
Beaufort Sea	2,080	1.8 × 10 ⁻⁷	7.1 × 10 ⁻⁴	6.4 × 10 ⁻⁷	6.0 × 10 ⁻⁴
Bering Sea	2,100	1.5 × 10 ⁻⁹	6.8 × 10 ⁻⁶	5.3 × 10 ⁻⁹	5.6 × 10 ⁻⁶
Chukchi Sea	2,080	5.6 × 10 ⁻⁸	3.2 × 10 ⁻⁴	2.0 × 10 ⁻⁷	2.7 × 10 ⁻⁴
Accidental release to the Ob River from Mayak					
Beaufort Sea	14		7.9 × 10 ⁻⁴		4.6 × 10 ⁻²
Bering Sea	25		4.1 × 10 ⁻⁶		3.0 × 10 ⁻⁴
Chukchi Sea	14		3.6 × 10 ⁻⁴		2.1 × 10 ⁻²
Chronic release to the Kara Sea from the Ob and Yenisey rivers					
Beaufort Sea	45				2.1 × 10 ⁻²
Bering Sea	70				2.0 × 10 ⁻⁴
Chukchi Sea	45				9.4 × 10 ⁻³

^aThe time of the peak dose refers to the number of years after a release occurs, except in the case of the time-varying release from the Kara Sea sources where the time of the peak is the year in which it occurs.

Releases from the Ob and Yenisey Rivers

Acute Releases

The acute release scenarios for radionuclide discharges to the Ob and Yenisey rivers consist of the year-long discharge of 1.4 PBq of ^{90}Sr and 24 TBq of ^{137}Cs , respectively, from the hypothesized failure of liquid-waste reservoirs at Mayak (see Section 2). Figures 3-11 and 3-12 show the resulting concentrations in the Chukchi, Beaufort, and Bering Seas for ^{90}Sr and ^{137}Cs , respectively. The peak concentrations of ^{137}Cs associated with the acute riverine releases, as summarized in Table 3-9, are comparable to the peak levels predicted for the time-varying release to the Kara Sea from the spent nuclear fuels. However, the predicted peak levels for ^{90}Sr are more consistent with the instantaneous release to the Kara Sea because it is comparable in magnitude (i.e., ~ 1 PBq).

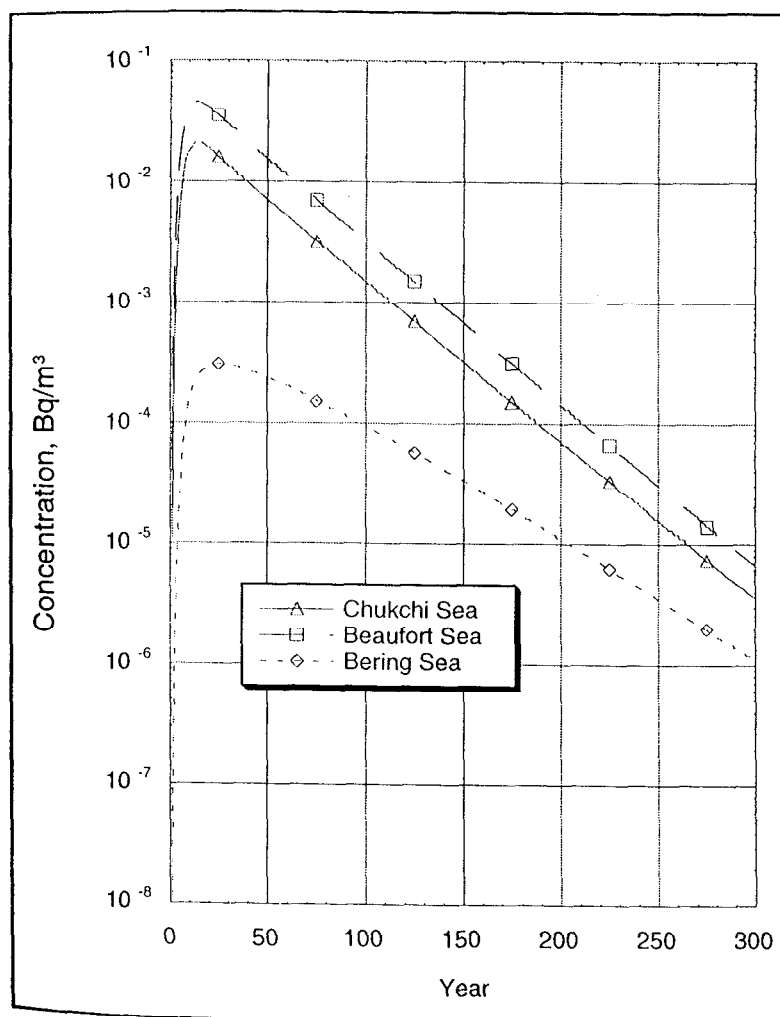


Figure 3-11. Concentrations of ^{90}Sr in the Beaufort, Bering, and Chukchi seas resulting from the accidental release of liquid waste from Mayak.

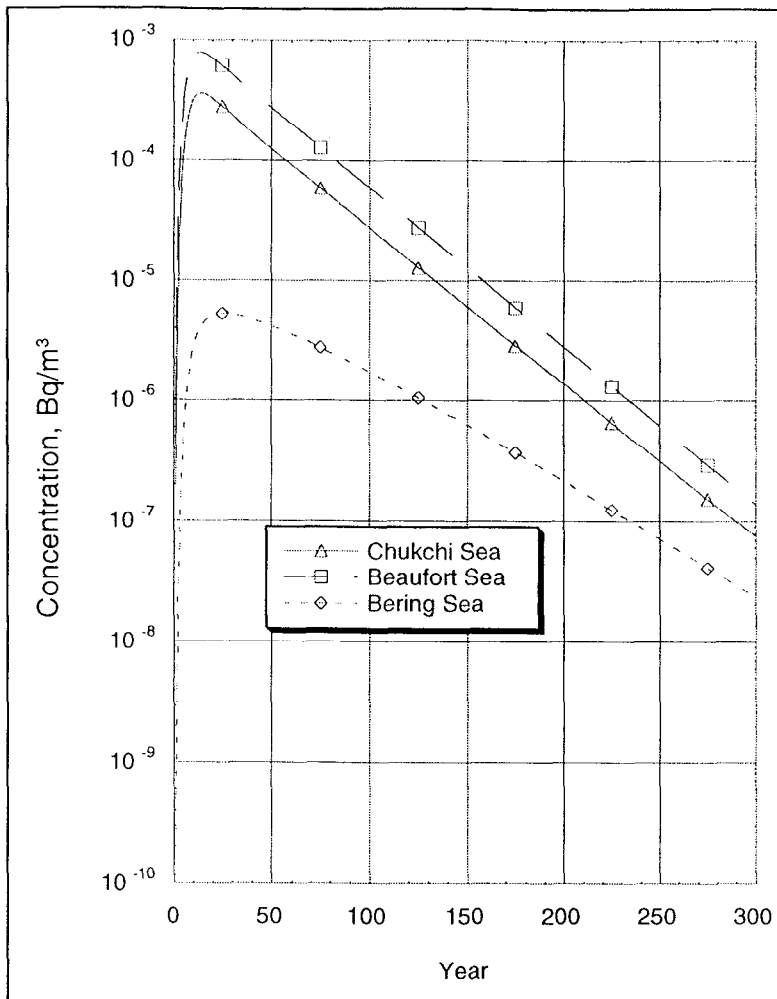


Figure 3-12. Concentrations of ^{137}Cs in the Beaufort, Bering, and Chukchi seas resulting from the accidental release of liquid waste from Mayak.

Chronic Release

The chronic release of ^{90}Sr is represented as a declining source term, based on an initial flux of 40 TBq/yr into the Kara Sea estuary. The peak concentrations in the Beaufort and Chukchi seas are comparable to the peak levels predicted for the instantaneous release of ^{90}Sr to the Kara Sea and for accidental discharge of radioactive liquid wastes at Mayak; however, the peaks occur after 45 years of release (see Figure 3-13).

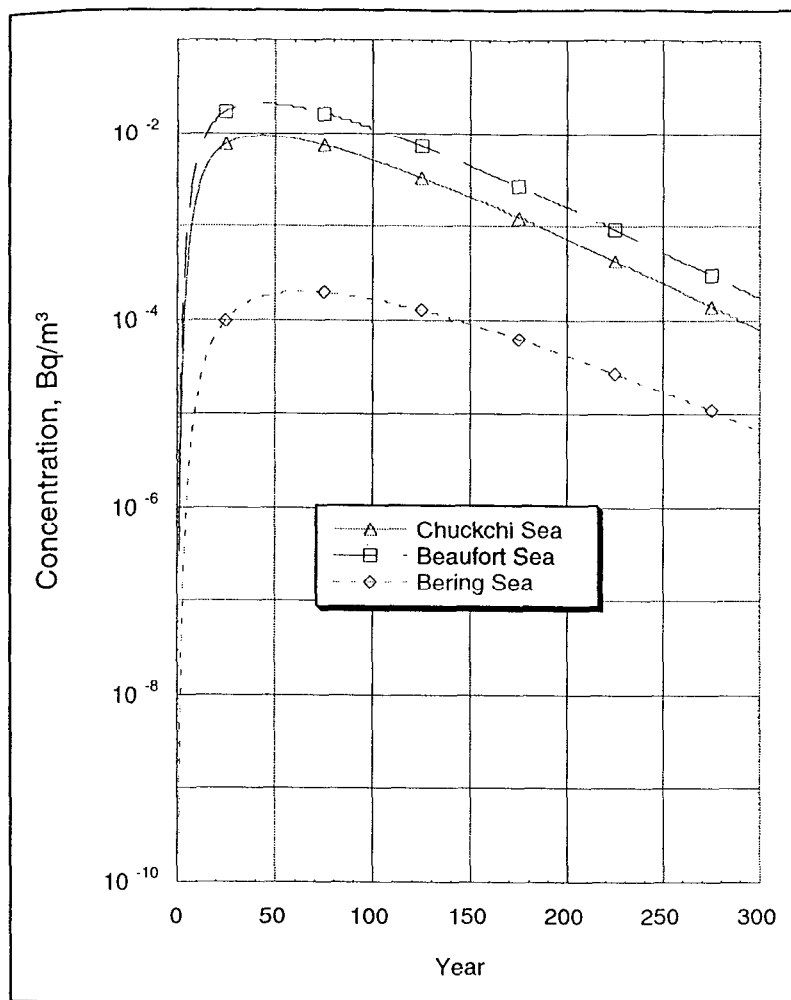


Figure 3-13. Concentrations of ^{90}Sr in the Beaufort, Bering, and Chukchi seas resulting from the chronic release of liquid wastes and watershed runoff into the Ob and Yenisey rivers.

3.3.5 Predicted Radionuclide Concentrations v. Historic Levels

Concentrations of ^{241}Am , ^{137}Cs , $^{239,240}\text{Pu}$, and ^{90}Sr in seawater have been measured since the early days of aboveground nuclear testing. As Section 2 discusses, nuclear fallout is a dominant source of fission products and actinides in the world's oceans. However, discharges from the nuclear reprocessing facility at Sellafield, U.K., also constitute an important source of such radionuclides for the Arctic Ocean because of ocean currents that transport reprocessing wastes from the North-east Atlantic Ocean to the Norwegian and Greenland seas. To compare the predicted concentrations of radionuclides in the Chukchi, Beaufort, and Bering seas with their historic levels in those seas and other locations, following is a brief review of pertinent data on the key radionuclides sampled in Arctic Ocean as well as source waters in the Atlantic and Pacific oceans.

Arctic Seas and Source Waters of the Atlantic and Pacific Oceans

Data on historic levels of fission products and actinides in Arctic waters adjacent to Alaska are sparse, but the available measurements do provide insights as to the sources of anthropogenic radionuclides in the Arctic seas. For example, an early study by Bowen and Sugihara (1964) showed that concentrations of ^{90}Sr in the Chukchi Sea gradually increased from 3.6 Bq/m³ in 1959 to about 9 Bq/m³ in 1962. They attributed the increase to an influx of ^{90}Sr through the Bering Strait that was derived from seawater contaminated with fallout from nuclear testing in the Pacific Ocean. Data from Medinets et al. (1992) show radiocesium burdens in surface and near-surface waters of the Bering and Chukchi seas in 1988 of 1.6 to 3.7 Bq/m³. Ellis et al. (1995) presented results of a polar cruise in 1994 that obtained seawater samples along a transect from the Chukchi Sea to the North Pole and then the Fram Strait. The greatest concentrations of ^{137}Cs were measured near the central portion of the Arctic Ocean (7 to 15 Bq/m³). In contrast, the lowest level (1.9 Bq/m³) was detected in the Chukchi Sea. Ellis et al. concluded that the elevated levels of ^{137}Cs were derived from reprocessing wastes from European nuclear facilities, while the low concentration of ^{137}Cs in the Chukchi Sea was from Pacific water flowing through the Bering Strait with ^{137}Cs derived from global fallout from nuclear weapons testing.

Because inflowing Pacific water basically controls the level of radionuclides in the Chukchi Sea, the RAIG reviewed data on the concentrations of fission products and actinides in the central and northern portions of the Pacific Ocean to estimate historic and modern levels in Alaskan waters. For example, the average concentrations of ^{241}Am , ^{137}Cs , $^{239,240}\text{Pu}$, and ^{90}Sr in seawater to a depth of 80 m at one location in the northern Pacific Ocean sampled by Livingston et al. (1985) in 1973 were 0.004, 6.1, 0.012, and 3.5 Bq/m³, respectively. In a later study involving ^{137}Cs , $^{239,240}\text{Pu}$, and ^{90}Sr in the central North Pacific, Nagaya and Nakamura (1984) reported that the average concentrations of those nuclides in surface waters of the 35° to 40° N latitudinal zone for the years 1980 and 1982 were 5.6, 0.038, and 4 Bq/m³. As a point of comparison, Nikitin et al. (1991) estimated that the average concentration of ^{137}Cs in the 0 to 250 m layer of the Arctic Ocean in the 81 to 83° N latitude zone was 8.5 Bq/m³ for the years 1985-1987. The 2.5 Bq/m³ increase over the ~6 Bq/m³ level estimated for the Chukchi Sea (from the measurements in Pacific waters noted above) undoubtedly is due to the influx of ^{137}Cs from the Sellafield reprocessing facility via the northeast Atlantic Ocean.

In contrast, the level of ^{137}Cs in the Chukchi Sea in 1962 would have been approximately 14 Bq/m³, calculated from the concentration of 9 Bq/m³ reported by Bowen and Sugihara (1964) and a multiplier of $\sim 1.5 \times$ concentration of ^{90}Sr (Volchok et al., 1971). Concentrations of ^{241}Am and ^{239}Pu in the early 1960s can also be estimated using ratios of the concentrations of those nuclides to the concentrations of ^{90}Sr in surface waters of the northern Pacific Ocean. The RAIG has calculated an average $^{239}\text{Pu}/^{90}\text{Sr}$ ratio of ~ 0.005 for these waters, based on the following set of concentration ratios: 0.0034 (for station at 50° 26.8' N 176° 35.0' W sampled in 1973; Livingston et al., 1985); 0.0075 (average for surface waters from stations 80-5, 80-6, and 80-8 sampled in 1980; Nagaya and Nakamura, 1984); and 0.0031 (for station at 30° 03' N 170° 03' W sampled in 1968, Miyake and Sugimura, 1976). The reconstructed ^{239}Pu concentration based on the measurement of ^{90}Sr for the 1962 sampling period is therefore 0.05 Bq/m³. The concentration of ^{241}Am is estimated to have been 0.009 Bq/m³, using a $^{241}\text{Am}/^{90}\text{Sr}$ ratio of about 0.001 determined from the station of Livingston et al. (1985). The RAIG estimates that the current concentration of ^{90}Sr in the Chukchi Sea is about 1 Bq/m³ (1.9 Bq/m³ \div 1.5), while the levels of ^{241}Am and $^{239,240}\text{Pu}$ would be about 0.001 and 0.005 Bq/m³, using the same ratios given above and the measured ^{137}Cs value of Ellis et al. (1995).

Comparisons with Predicted Levels

Our estimates of the existing and historic concentrations of ^{241}Am , ^{137}Cs , ^{239}Pu , and ^{90}Sr in Alaskan waters are all well above the levels associated with the peak doses for the different source-term scenarios, as summarized in Table 3-9. The highest predicted levels in Alaskan waters are associated with instantaneous releases of radionuclides from the nuclear wastes in the Kara Sea and from liquid-waste reservoirs at Mayak. Existing levels of ^{90}Sr are more than 20 times higher than predicted peak concentrations, and concentrations in the 1960s are about another factor of 10 higher. The highest predicted concentration of ^{137}Cs is 0.032 Bq/m^3 in the Beaufort Sea after an instantaneous release to the Kara Sea. This level is much lower than the 2 Bq/m^3 of ^{137}Cs measured in the 1990s. The slow, time-varying release of nuclides from Kara Sea wastes from dissolution/corrosion processes is a more realistic source-term scenario, and the resulting concentrations for the four nuclides are far below both the historic and existing levels as well as those predicted for the unlikely instantaneous release case.

3.4 SUMMARY

- A compartmental modeling approach was used to simulate the transport of radionuclides derived from the Kara Sea nuclear wastes and riverine sources to Alaskan waters. Water flows between compartments were estimated using a coupled ice-ocean circulation model. Radionuclide losses within a given compartment occur via sedimentation and radioactive decay. The model is capable of simulating discrete as well as time-varying releases of radionuclides to ocean waters over long periods (decades or centuries).
- Site-specific data on sediment/water distribution coefficients (K_d s) for ^{241}Am , ^{137}Cs , ^{239}Pu , and ^{90}Sr indicate that the K_d s based on Kara Sea sediments are generally lower than default values used for coastal waters. Sediment loadings in the coastal portions of the Arctic Ocean are around 1 mg/L , whereas in the central portion of the basin the levels are considerably lower, based on limited measurements. Because of the reduced K_d s and low particle loadings in the Arctic Ocean, water currents rather than sedimentation processes dominate nuclide transport.
- The role of ice formation and movement has been identified as a potential transport mechanism for radionuclide contaminants present in shallow areas of the Kara Sea. Our screening-level analyses indicate that the transport of radionuclides in coastal waters to the Arctic Ocean is probably a more dominant transport mechanism for such contaminants because the transport capacity of coastal water currents is greater than the capacity associated with ice and entrained sediment.
- The RAIG conducted a bench-marking exercise in which the team compared the results of the RAIG compartmental model with a modified version of one developed by Nielsen et al. (1995) to assess radionuclide transport in the Arctic Ocean. Both models provided similar results for ^{137}Cs and ^{90}Sr , however, the concentrations predicted for ^{239}Pu and ^{241}Am in Alaskan waters based on their release into the Kara Sea were much lower in the Nielsen et al. model than in the RAIG model. This was attributed to increased scavenging of those particle-reactive nuclides in coastal compartments because of the K_d s used and the structure of the coastal compartments in the Nielsen et al. model.

- Data on the concentrations of the four nuclides in Alaskan waters indicate that the highest levels occurred in the 1960s as a result of global nuclear fallout. The predicted concentrations of the radionuclides in the Beaufort, Bering, and Chukchi seas were much lower than either historic or currents levels. This is not surprising given the 3,700 km transport distance between Novaya Zemlya and the north slope of Alaska. The highest predicted concentration of ^{137}Cs was 0.032 Bq/m³ in the Beaufort Sea after an instantaneous release to the Kara Sea from nuclear wastes. This level is much lower than the 2 Bq/m³ of ^{137}Cs measured in the 1990s. A more realistic release scenario, in which nuclides are released slowly to the Kara Sea as a result of corrosion and dissolution processes, results in predicted concentrations that are much lower.
- The RAIG model provides adequate detail for the assessment of potential risks to Alaska. It uses a large averaging near the sources of radionuclide release, and for this reason would not be as useful for resolving impacts in the immediate vicinity of the waste-disposal sites.